

This is an Accepted Manuscript for *Journal of Glaciology*. Subject to change during the editing and production process.

DOI: 10.1017/jog.2023.10

# Observing glacier dynamics with low-cost, multi-GNSS

## positioning in Victoria Land, Antarctica

Holly STILL,<sup>1</sup> Robert ODOLINSKI,<sup>1</sup> M. Hamish BOWMAN,<sup>2</sup> Christina HULBE<sup>1</sup> David J.

PRIOR<sup>2</sup>

<sup>1</sup>*School of Surveying, University of Otago, Dunedin, NZ*

<sup>2</sup>*Department of Geology, University of Otago, Dunedin, NZ*

*Correspondence:* Holly Still <holly.still@postgrad.otago.ac.nz>

### ABSTRACT.

This study examines the performance of low-cost, low-power GNSS positioning systems for glacier monitoring in high-latitude environments. We compare the positioning performance of co-located low-cost u-blox ZED-F9P GNSS units (a few hundred USDs) and survey-grade Trimble R10 units (>\$10,000 USD) under stationary (on land) and dynamic (on glacier) conditions near Terra Nova Bay, Antarctica. Low-cost and survey-grade systems yield almost identical error magnitudes under short (3 m), medium (34 km) and long (390 km) baseline kinematic-positioning scenarios. We further examined the efficacy of low-cost GNSS for glaciological applications by installing four u-blox and two Trimble receivers on Priestley Glacier to observe tide-modulated ice flexure. All receivers successfully detected subtle tidal oscillations with amplitudes <3 cm, consistent with the predicted phasing from a tide model. These experiments offer a strong rationale for the widespread use of low-cost receivers to expand and densify GNSS monitoring networks, both in Antarctica and in glaciated regions worldwide.

### 1 INTRODUCTION

Ice displacement and velocity are fundamental measurements used in glaciology to investigate ice mechanics and to constrain ice flow models. Observations of ice displacement are often obtained *in situ* using Global Navigation

This is an Open Access article, distributed under the terms of the Creative Commons Attribution-NonCommercial-NoDerivatives licence (<http://creativecommons.org/licenses/by-nc-nd/4.0/>), which permits non-commercial re-use, distribution, and reproduction in any medium, provided the original work is unaltered and is properly cited. The written permission of Cambridge University Press must be obtained for commercial re-use or in order to create a derivative work.

26 Satellite Systems (GNSS), which can provide high-precision horizontal and vertical positioning and precise timing  
27 information. Applications in Antarctica include the measurement of ice velocity and strain rate (Hulbe and Whillans,  
28 1994; Minowa and others, 2019; Klein and others, 2020), observation of vertical land motion (Thomas and others,  
29 2011; Zanutta and others, 2017; King and others, 2022), validation of satellite and radar ice altimetry data (Schröder  
30 and others, 2017; Brunt and others, 2019), and mapping of ice surface topography and surface elevation change (Hulbe  
31 and Whillans, 1997; Spikes and others, 2003; Richter and others, 2014). GNSS positioning is used to provide location  
32 and contextual information for transmitters and receivers used for geophysical remote-sensing techniques, including  
33 radar sounding (Horgan and others, 2017; Pratap and others, 2022), passive and active-source seismic sounding  
34 (Minowa and others, 2019; Huang and others, 2022), and gravity measurements (Zanutta and others, 2018). It  
35 is used to locate sample collection sites, including ice cores and ice-anchored moorings (Arzeno and others, 2014;  
36 Thomas and others, 2021). Many of these applications require (or could benefit from) a network of multiple GNSS  
37 devices deployed, yet this is costly and logistically challenging in polar environments.

38 Glaciological applications typically use geodetic or survey-grade GNSS receivers and antennas (e.g., Siegfried and  
39 others, 2016; Cooley and others, 2019; Brunt and others, 2019; Still and others, 2022). These systems are robust,  
40 reliable, and can provide dual or triple frequency, multi-GNSS data at a high rate ( $\geq 1$  Hz), leading to centimetre-level  
41 horizontal and vertical precision under ideal conditions. However, these systems are also expensive. State-of-the-  
42 art survey-grade GNSS receiver and antenna systems can retail for  $\sim \$30,000$  USD, and refurbished last-generation  
43 systems were available for  $\sim \$5,000$  to  $\$10,000$  USD at the time of writing (AllTerra, 2023). High equipment costs  
44 can be prohibitive to scientific discovery, limiting the concurrent deployment of multiple GNSS receivers over large  
45 areas of interest and restricting access to users with well-financed research programs (e.g., Chagas, 2018; Oellermann  
46 and others, 2022). Additional limitations of survey-grade receivers for deployment in remote environments include  
47 high rates of power consumption, the size and weight of receivers and antennas, and the weight of battery banks  
48 needed for multi-day installations (Willis, 2008; Jones and Rose, 2015; Jones and others, 2016).

49 Low-cost, mass-market GNSS chip devices – a relatively new and rapidly developing technology – are a promising  
50 alternative to the GNSS units typically used in glacier studies. These low-cost systems retail for less than 10%  
51 of the cost of survey-grade alternatives (AllTerra, 2023; U-blox, 2023). Coupled with a low-cost antenna and data  
52 logger, low-cost GNSS receivers are light and compact, with relatively low power consumption (e.g., den Ouden and  
53 others, 2010; Jones and others, 2016). The key difference between low-cost and survey-grade hardware lies in the  
54 quality of the receiver electronics. Electronic components generate internal receiver noise that affects the continuous  
55 tracking of satellite signals and ambiguity fixing, particularly when GNSS signals are weak. Nonetheless, low-cost

receivers and antennas can achieve centimetre-level precision by tracking multiple GNSS satellite constellations (e.g., GPS, GLONASS, Galileo, Beidou, QZSS) at two or more carrier frequencies (Odolinski and Teunissen, 2016, 2020). The low-cost u-blox ZED-F9P GNSS receiver, for example, has a specified real time kinematic (RTK) positioning accuracy of 1 cm + 1 ppm CEP over a 1 km baseline in optimal conditions (U-blox, 2022c). In practice, the positioning performance depends on baseline length (the distance between a reference station and moving GNSS receiver), satellite-receiver geometry, antenna and receiver hardware design, atmospheric conditions, and multipath interference errors (Odijk and Wanninger, 2017, pg. 770-773), all of which are relevant to polar applications. The performance of readily-available u-blox ZED-F9P receivers is investigated here as a low-cost solution for glacier monitoring.

The precision and reliability of low-cost GNSS receivers has been evaluated for short baseline, static and dynamic positioning at mid to low latitudes (e.g., Odolinski and Teunissen, 2016; Nie and others, 2020; Xue and others, 2022). Similar performance comparisons between low-cost and survey-grade systems have not been conducted in high-latitude, glaciated environments. Of relevance to polar environments where permanent GNSS reference stations are sparse, Odolinski and Teunissen (2020) show that the positioning performance of u-blox ZED-F9P receivers is competitive with a survey-grade system in a long-baseline (112.9 km), kinematic-positioning configuration. Performance evaluations of u-blox receivers in geophysical monitoring contexts have also yielded millimetre-level precision for continuous tectonic motion (Tunini and others, 2022) and landslide detection (Šegina and others, 2020; Notti and others, 2020). In controlled, short-baseline (<100 m) RTK positioning experiments, u-blox ZED-F9P receivers paired with low-cost antennas could detect mechanically-induced horizontal displacements as small as 10 mm (Hamza and others, 2020). All of these results suggest that the measurement precision needed for glacier mechanics studies is possible with this equipment, and for this reason, u-blox GNSS hardware is evaluated in the present study.

Polar environments present challenges, limitations, and sources of error that can affect the positioning performance of both low-cost and survey-grade GNSS equipment. At high latitudes, maximum satellite elevations are lower in the sky, with no satellites passing directly overhead (King and others, 2000; Zhang and others, 2020; Di and others, 2022). This weaker satellite-receiver geometry can lead to an unfavourable vertical dilution of precision and larger vertical positioning errors (Hugentobler and Montenbruck, 2017; Alkan and others, 2022). A second source of error, multipath interference, occurs when transmitted signals are deflected off objects before reaching the receiver. Highly reflective snow and ice surfaces may amplify multipath errors, particularly when satellites are at low elevations above the horizon (e.g., Wanninger and May, 2001; Nievinski and Larson, 2014). A third source of error originates from the degradation of GNSS signals due to geomagnetic and ionospheric storms. These space weather disturbances have a

86 greater intensity at high latitudes, near the magnetic poles (Skone and others, 2001; Doherty and others, 2003; Linty  
87 and others, 2018; Nie and others, 2022; Paziewski and others, 2022). Altogether, these error sources and the presence  
88 of low elevation satellites can affect positioning performance by decreasing the GNSS receiver signal-to-noise ratio  
89 and increasing the frequency of cycle slips, a temporary loss-of-lock on a satellite (Dabovic and others, 2020; Di and  
90 others, 2022).

91 Performance evaluations of GNSS receivers are often undertaken in controlled, open-sky environments with  
92 favourable conditions to achieve optimal precision and accuracy. These conditions can include: a satellite–receiver  
93 geometry that minimises positioning errors, calm ionospheric conditions, short baselines (<50 km), and mitigation  
94 of low-elevation multipath errors. This study evaluates low-cost GNSS positioning performance in a high latitude,  
95 glaciated environment in Antarctica under challenging conditions, including medium to long baselines, varying iono-  
96 spheric conditions, a glacier-valley site with some loss of sky view, a highly reflective snow or ice surface, sub-zero  
97 temperatures and differing receiver and antenna models for the base station and rover. An important objective is to  
98 evaluate whether the performance of low-cost GNSS is suitable for glaciological applications that require centimetre-  
99 level precision (e.g., the detection of velocity variability over timescales of hours to days).

## 100 1.1 Objectives

101 This study analyses the performance of low-cost, low-power GNSS positioning for glacier and ice-sheet monitor-  
102 ing applications in high-latitude environments. We compare the performance of u-blox ZED-F9P GNSS receivers  
103 (<\$300 USD) and survey-grade Trimble R10 receivers (>\$10,000 USD) under stationary (on land) and dynamic (on  
104 glacier) conditions near Terra Nova Bay, Antarctica. In each experiment, u-blox and Trimble receivers were installed  
105 alongside each other to record positions simultaneously under the same satellite geometry and environmental condi-  
106 tions. The u-blox receivers were paired with both low-cost patch antennas and standard surveying antennas while  
107 the Trimble R10 receivers were used with their integrated antenna.

108 Three experiments were performed. The first experiment compares and evaluates performance under stationary  
109 conditions on stable ground near Mario Zucchelli Station in Terra Nova Bay, Antarctica (Fig. 1). This short  
110 baseline (3 m) experiment establishes the optimal expected performance of the receivers at a high-latitude site. The  
111 second experiment compares and evaluates the performance under dynamic conditions on Priestley Glacier. Three  
112 GNSS units (2 u-blox, 1 Trimble) were installed alongside each other on an advecting ice surface. We evaluate  
113 the kinematic positioning solutions for both medium (34 km) and long baselines (390 km). The third experiment  
114 evaluates performance in a realistic glacier monitoring context: observing the tidal flexure of Priestley Glacier's left

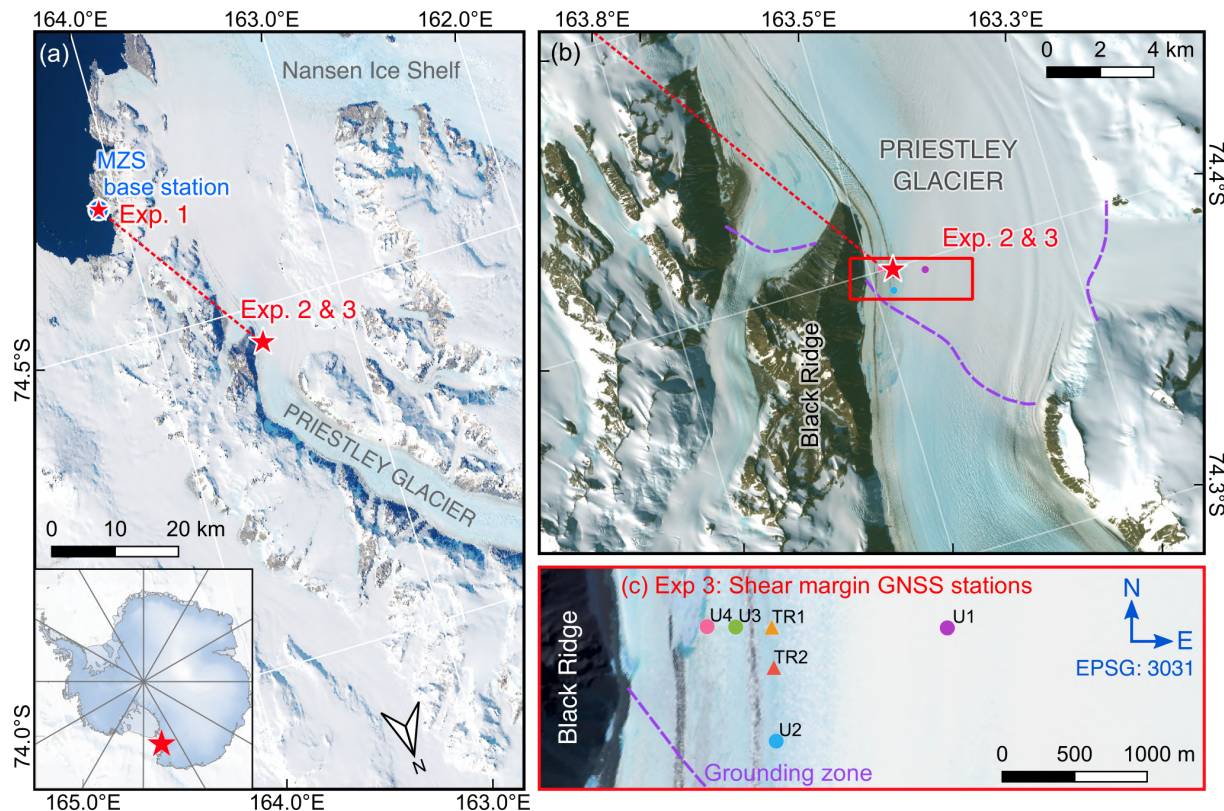


**Fig. 1.** Site map of GNSS experiments conducted near Terra Nova Bay in the Ross Sea region, Antarctica. Map (a): the location of the stationary GNSS experiment (Experiment 1) at Mario Zucchelli Station (Mzs), and the dynamic GNSS experiments on Priestley Glacier (Experiments 2 and 3). Map (b): the field site near Priestley Glacier's left lateral margin, approximately 1 km downstream from the grounding zone. Map (c): the locations of u-blox (U) and Trimble (TR) GNSS stations installed across the shear margin (Experiment 3). The estimated location of the grounding zone is from Rignot and others (2016) and the basemaps contain modified Sentinel-2, 10 m resolution imagery acquired on December 18, 2022, courtesy of the European Space Agency.

115 lateral shear margin. Six GNSS units (4 u-blox, 2 Trimble) were installed in across- and along-flow transects near  
116 the margin of Priestley Glacier (Fig. 1). GNSS positioning performance is evaluated in terms of precision, the  
117 repeatability or variability of a measured quantity.

118 Single-baseline kinematic positioning solutions are used in the present work. That is, we determine the trajectory  
119 of a moving GNSS antenna (the ‘rover’) relative to a single stationary base station receiver. This is a relative  
120 positioning technique and the ‘baseline’ is the distance between the rover and a base station. The technique requires  
121 simultaneous observations from the two receivers, one of which is installed on stationary terrain. Relative positioning  
122 eliminates satellite and receiver clock errors, and reduces errors associated with satellite orbits, ionospheric, and  
123 tropospheric delays. Centimetre-level or better precision is feasible providing that integer ambiguity resolution is  
124 achieved.

125 An alternative positioning method, precise point positioning (PPP), requires the deployment of only a single  
126 GNSS receiver (Zumberge and others, 1997; Kouba and Héroux, 2001). PPP is commonly used in remote polar  
127 environments where logistical difficulties or lack of access to stationary terrain are barriers to the installation of  
128 temporary base stations (King and Aoki, 2003; King, 2004). Permanent GNSS reference stations in Antarctica are  
129 sparse, distributed near coastlines, and may be located hundreds of kilometres away from field sites. Both single-  
130 baseline kinematic positioning and PPP have produced centimetre-level precision in Antarctica, using survey-grade  
131 equipment (Hulbe and others, 2016; Schröder and others, 2017; Brunt and others, 2019; Still and others, 2022; Alkan  
132 and others, 2022). The quality of a PPP solution, however, depends on precise orbit and clock products, and the  
133 convergence time (hours rather than minutes) is significantly longer compared to relative positioning methods. If the  
134 goal is to achieve very precise 3D positions and velocities, a single-baseline kinematic positioning solution is expected  
135 to be the best-performing technique in a short to medium baseline configuration (i.e., less than 100 km between base  
136 station and rover).

## 137 2 METHODS

### 138 2.1 Low-cost GNSS instrumentation

139 Each low-cost GNSS installation includes a receiver, antenna, data logger and power source (two 10 W, 12 V solar  
140 panels and a 12 V, 18 A h SLA battery) (Table 1). The u-blox ZED-F9P GNSS receiver module is capable of tracking  
141 GPS (L1/L2), GLONASS (L1/L2), Galileo (E1/E5b), Beidou (B1/B2), and QZSS (L1/L2) systems and frequencies  
142 (U-blox, 2022c). The ZED-F9P module operates over a wide temperature range ( $-40^{\circ}\text{C}$  to  $85^{\circ}\text{C}$ ) and the rate of  
143 power consumption is relatively low (0.57 W for the u-blox ZED-F9P module + patch antenna + Arduino Cortex

144 M0 logger, versus 1.25 W for a Trimble R10 system, and 3.67 W for a Trimble NetR9 system). The receiver is  
145 configured to log all available satellites and frequencies at 1 Hz using the software U-center v22.07 (U-blox, 2022b).  
146 RXM-RAWX messages (raw carrier phase, pseudorange, Doppler and signal quality information) and RXM-SFRBX  
147 messages (broadcast navigation data) are enabled and the raw binary u-blox files are stored with an Arduino data  
148 logger to micro SD card.

149 Two low-cost multiband antenna models are trialled with the u-blox receivers: the u-blox ANN-MB patch antenna  
150 (U-blox, 2022a) and an Eltehs multiband (ELT0123) standard surveying antenna (GNSS OEM, 2023) (Table 1).  
151 Patch antennas are designed to attach to flat surfaces and have magnetic bases for this purpose. We attach our patch  
152 antennas to 0.12 m diameter circular steel plates fabricated for these experiments. The plates act as a ground plane  
153 that reduces multipath interference for the otherwise exposed antennas (U-blox, 2019; Punzet and Eibert, 2023). In  
154 Experiments 1 and 2, the ground plates are bolted onto tripods. In Experiment 3, the plates are attached to uPVC  
155 glacier stakes frozen into the ice. The u-blox ANN-MB patch antenna has the advantage of a light and compact  
156 form, with the limitation of a poorer gain performance (28 dB, versus 50 dB for the Trimble R10 antenna). The  
157 gain pattern of a higher-quality antenna is optimised to suppress low elevation GNSS signals, including multipath  
158 interference (Maqsood and others, 2017).

## 159 2.2 Low-cost and survey-grade GNSS data processing

160 The first processing step involves a conversion from the proprietary u-blox and Trimble raw data file formats to  
161 standard RINEX 3.03 (Receiver Independent Exchange) files. U-blox data streams are converted using open-source  
162 RTKLIB tools (Takasu and Yasuda, 2009). Trimble observation files were converted using the Trimble ‘Convert to  
163 RINEX’ utility, version 3.1.4.0. GNSS stationary and dynamic observations are post-processed using the RTKPOST  
164 module within RTKLIB v2.4.3 b34 (Takasu and Yasuda, 2009; Takasu, 2013).

165 Multi-GNSS (GPS, GLONASS, Galileo, Beidou and QZSS) pseudorange and carrier phase measurements are  
166 post-processed in kinematic mode using RTKLIB. A satellite elevation cut-off angle of 15° is applied to mitigate  
167 low-angle multipath or atmospheric errors. Solutions are computed at a 1 second measurement interval for short  
168 baselines (Experiment 1) to demonstrate that the low-cost system is capable of high-rate (1 Hz) data logging in  
169 this environment. For medium and long baselines (Experiments 2 and 3), solutions are computed at a 10 second  
170 measurement interval to avoid reported time correlations of several seconds in the code observations of u-blox M8T  
171 and F9P receivers (Odolinski and Teunissen, 2017b, 2020), which if neglected, may affect the positioning results.  
172 This is particularly true for medium and long baselines when relative atmospheric delays enter the model (Odolinski,

**Table 1.** Specifications of the GNSS receiver and antenna hardware evaluated in each experiment. All frequency bands supported by the GNSS receivers are listed. Frequencies in bold font are used in the three experiments for a fairer comparison between u-blox and Trimble systems. Power consumption estimates are from measurements rather than manufacturer specifications. Low-cost equipment prices are from the GNSS OEM Store (<https://gnss.store/content/4-about-us>) and survey-grade equipment pricing is from AllTerra (2023).

Receiver/antenna	u-blox ZED-F9P + multiband patch antenna	u-blox ZED-F9P + multiband surveying antenna	Trimble R10 (integrated antenna)
Systems and frequencies (receiver)	GPS: <b>L1, L2</b> GLO: <b>L1, L2</b> GAL: <b>E1, E5b</b> BDS: <b>B1, B2</b> QZSS: <b>L1, L2</b>	GPS: <b>L1, L2</b> GLO: <b>L1, L2</b> GAL: <b>E1, E5b</b> BDS: <b>B1, B2</b> QZSS: <b>L1, L2</b>	GPS: <b>L1, L2, L5</b> GLO: <b>L1, L2, L3</b> GAL: <b>E1, E5b, E5a, E6</b> BDS: <b>B1, B2, B3</b> QZSS: <b>L1, L2, L5</b>
Dimensions (receiver)	17.0 × 22.0 × 2.4 mm	17.0 × 22.0 × 2.4 mm	119 × 119 × 136 mm
Dimensions (antenna)	60.0 × 82.0 × 22.5 mm	160.0 × 160.0 × 66.5 mm	n/a
Weight (receiver)	< 100 g	< 100 g	1.12 kg
Weight (antenna)	173 g	400 g	n/a
Operating temp (receiver)	-40 °C to +85 °C	-40 °C to +85 °C	-40 °C to +65 °C
Operating temp (antenna)	-40 °C to +85 °C	-40 °C to +70 °C	n/a
Receiver price	\$187 USD	\$187 USD	> \$10,000 USD (used)
Antenna price	\$90 USD	\$199 USD	n/a
Power usage of GNSS system	0.57 W	0.65 W	1.25 W
Positioning accuracy (horiz)	0.01 m + 1 ppm CEP	0.01 m + 1 ppm CEP	0.008 m + 1 ppm RMS (RTK)
Antenna gain	28 dB	38 dB	50 dB
Experiment 1 (Fig. 2)	Rover + base station	n/a	Rover + base station
Experiment 2 (Fig. 6)	Rover (Ub2)	Rover (Ub1)	Rover (Tr1)
Experiment 3 (Fig. 1c)	Rover (Ub3, Ub4)	Rover (Ub1, Ub2)	Rover (Tr1, Tr2)

173 2012).

174 Base station and rover pairs are listed in Table 2 and kinematic processing techniques and parameters are sum-  
175 marised in Table 3. RTKLIB configuration settings are modified to improve the solutions for short, medium, or  
176 long baselines (e.g., Odolinski and others, 2015b). Identical processing settings are applied to each base–rover pair  
177 within each experiment and are not modified to suit a low-cost or survey-grade receiver or antenna, ensuring a  
178 fair performance comparison between the different solutions. Antenna phase centre offset (PCO) and phase centre  
179 variations (PCV) from the IGS14 antenna calibration database (IGS14.atx) are defined in RTKLIB for survey-grade  
180 Trimble observations. PCOs and PCVs are ignored for the low-cost multiband surveying antenna and ANN-MB  
181 patch antenna, although providing these values for low-cost cost antenna models may reduce error magnitudes by  
182 a few millimetres (Krietemeyer and others, 2022). Daily multi-GNSS broadcast ephemeris files (the BRDM00DLR\*  
183 product) (Steigenberger and Montenbruck, 2020) from the CDDIS GNSS data archive (Noll, 2010) are used for short  
184 and medium baseline tests. Final multi-GNSS orbit and clock information (GFZ0OPSFIN\* products) from the GFZ  
185 Analysis Centre (Männel and others, 2022; Montenbruck and others, 2017) are used for the long baseline (390 km)  
186 test because satellite orbit errors enter the single-baseline positioning model as the baseline increases. Output posi-  
187 tions are provided as WGS84 latitude, longitude and ellipsoidal height. Coordinates are transformed to the Antarctic  
188 Polar Stereographic coordinate system (EPSG:3031). Time series position data are presented with the mean position  
189 for each station removed.

190 Smoothing or filtering techniques are often applied to processed GNSS time series to remove unrealistic peaks  
191 and high frequency noise associated with multipath interference. In Experiment 3 (Fig. 1c), in which the objective  
192 is to observe ice flexure and tidal modulation of ice velocity, outliers are removed with a three-hour moving median  
193 filter to prevent unrealistic peaks in the horizontal and vertical position time series. This method defines outliers as  
194 points that fall beyond a threshold of three scaled median absolute deviations from the sliding median. No filtering,  
195 smoothing or outlier detection methods are applied to the solutions in Experiments 1 and 2 (Section 1.1). GNSS  
196 data are presented ‘as is’ for the comparisons between low-cost and survey-grade receivers.

### 197 3 EXPERIMENT 1: STATIONARY, SHORT-BASELINE POSITIONING

198 This experiment quantifies the uncertainty of GNSS positions obtained with low-cost u-blox systems and directly com-  
199 pares the performance of u-blox and Trimble receivers under the same environmental conditions. In a short-baseline  
200 positioning configuration, ionospheric and tropospheric errors, and satellite clock and orbit errors are negligible. This  
201 stationary, short-baseline experiment therefore demonstrates the optimal expected performance of the low-cost GNSS

**Table 2.** Summary of GNSS positioning experiments conducted at Mario Zucchelli Station (MZS) and on Priestley Glacier (PG). Experiment sites are mapped in Fig. 1.

<b>Low-cost u-blox versus Trimble comparisons</b>						
	Baseline	Rover receiver + antenna	Base receiver + antenna	Duration	Rover site	Section
<b>Experiment 1</b> (Stationary)	3.5 m	u-blox F9P + patch	u-blox F9P + patch	13 hrs	MZS	3.1
	3.5 m	Trimble R10	Trimble R10	13 hrs	MZS	
<b>Experiment 2</b> (Dynamic, medium baseline)	34 km	u-blox F9P + patch	Trimble NetR9 + Zephyr	15 hrs	PG	4.1
	34 km	u-blox F9P + surveying	Trimble NetR9 + Zephyr	15 hrs	PG	
	34 km	Trimble R10	Trimble NetR9 + Zephyr	15 hrs	PG	
<b>Experiment 2</b> (Dynamic, long baseline)	390 km	u-blox F9P + patch	Trimble Alloy + Zephyr 3	15 hrs	PG	4.2
	390 km	u-blox F9P + surveying	Trimble Alloy + Zephyr 3	15 hrs	PG	
	390 km	Trimble R10	Trimble Alloy + Zephyr 3	15 hrs	PG	
<b>Application: kinematic positioning to monitor tidally-modulated ice flexure</b>						
	Baseline	Rover receiver + antenna	Base receiver + antenna	Duration	Rover site	
<b>Experiment 3</b> (Dynamic)	34 km	Trimble R10	Trimble NetR9 + Zephyr	8.5 days	PG	5
	34 km	Trimble R10	Trimble NetR9 + Zephyr	7 days	PG	
	34 km	u-blox F9P + patch	Trimble NetR9 + Zephyr	4 days	PG	
	34 km	u-blox F9P + patch	Trimble NetR9 + Zephyr	4 days	PG	
	34 km	u-blox F9P + surveying	Trimble NetR9 + Zephyr	3 days	PG	
	34 km	u-blox F9P + surveying	Trimble NetR9 + Zephyr	3 days	PG	

**Table 3.** RTKLIB configuration settings for post-processing of u-blox and Trimble position time series.

Setting	Short baseline	Medium baseline	Long baseline
Dynamic model for positions	None (kinematic)	None (kinematic)	None (kinematic)
Constellations	G, R, E, C, J	G, R, E, C, J	G, R, E
Frequencies	L1+L2	L1+L2	L1+L2
Filter type	Forward	Forward	Forward
Elevation mask	15°	15°	15°
Ionospheric modelling	Can be ignored	Estimate slant total electron content (STEC)	Estimate STEC
Wet tropospheric delay estimation	None	None	Estimate zenith tropospheric delay (ZTD) (mapping function: Niell)
Satellite Ephemeris/Clock	Broadcast	Broadcast	Precise
Dynamic model for ambiguities	Time constant	Time constant	Time constant

202 devices for polar applications.

203 The stationary comparisons of low-cost u-blox and survey-grade Trimble receivers were conducted at Mario Zuc-  
 204 chelli Station, a coastal research station located on a granite promontory in Terra Nova Bay ( $74.6954^{\circ}$  S,  $164.0962^{\circ}$  E).  
 205 Four GNSS units (2 low-cost u-blox F9P receivers and 2 survey-grade Trimble R10 receivers) were deployed in a base  
 206 station and rover pair, on stationary ground, with a short baseline of 3.5 m (Fig. 2). Receivers and antennas were  
 207 installed approximately 300 m up-slope from Mario Zucchelli Station to maximise sky view and avoid interference  
 208 from buildings. Both u-blox receivers were equipped with ANN-MB patch antennas and ground plates. The Trimble

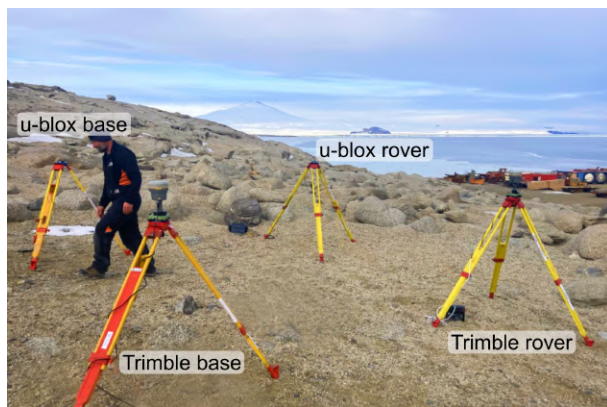


**Fig. 2.** Low-cost u-blox and survey-grade Trimble receivers and antennas in a short-baseline (3.5 m) configuration near Mario Zucchelli Station in Terra Nova Bay, Antarctica (Experiment 1).

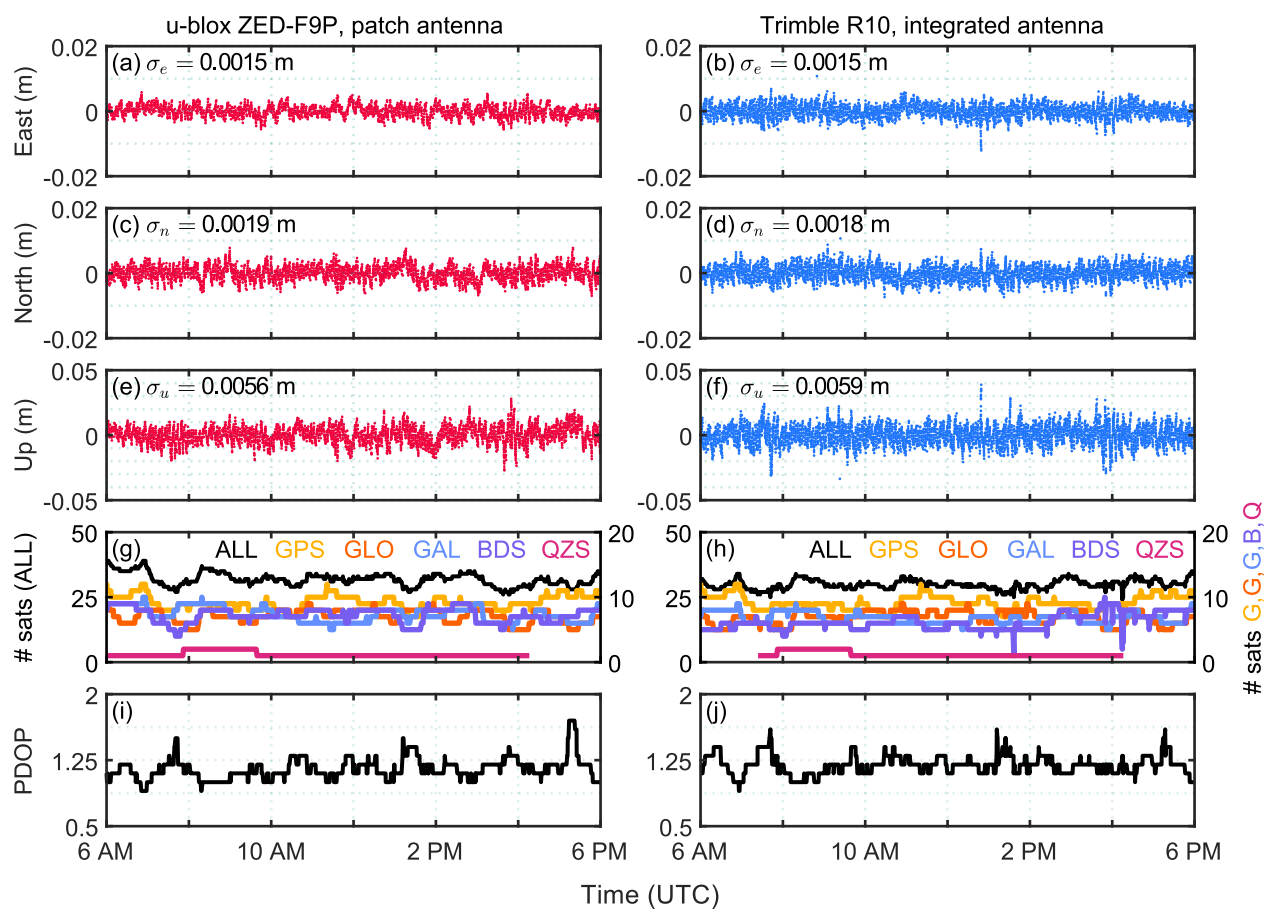


**Fig. 3.** Short baseline, stationary positions recorded with u-blox and Trimble GNSS stations over a 12 hour observation period on 16 November, 2022 (Experiment 1). East and north components of position correspond to the horizontal axes of the Antarctic Polar Stereographic coordinate system (EPSG:3031), with the mean position removed.  $n = 43,200$  epochs are included in each time series (1 Hz sample rate).  $\sigma$  is one standard deviation. The PDOP is the 3D position dilution of precision. Note the change in  $y$ -axis limits from  $\pm 2$  cm for the horizontal components to  $\pm 5$  cm for the vertical component.

R10 hardware consists of a receiver and ultra-compact Zephyr antenna within a single unit. Positions logged during the final 12 hours of the experiment, 0600 to 1800 hours (UTC) on 16 November, 2022, are analysed here. Positioning performance is evaluated in terms of the standard deviation for each component of position (east, north, up), and the 2D (horizontal) and 3D (horizontal and vertical) root mean square (RMS) errors, a collective measure of the difference between observed and expected positions. Statistics for each experiment are presented in Table 4.

### 3.1 Short-baseline positioning performance

The satellite visibility and geometry together affect the precision of the horizontal and vertical positions. Both u-blox and Trimble systems were configured to track five satellite systems visible in Antarctica (GPS, GLONASS, Galileo,

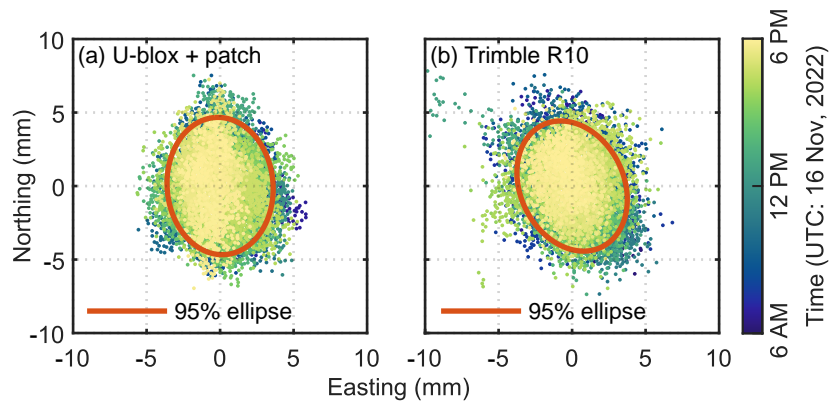


**Fig. 4.** Horizontal positions and 2D 95% confidence ellipses for the u-blox and Trimble position time series. Confidence ellipses are computed from  $n = 43,200$  positions obtained over 12 hours on 16 November, 2022. ‘North’ corresponds to grid north and the coordinate system is the same as in Fig. 3.

Beidou, QZSS). With an elevation cutoff angle of  $15^\circ$ , the u-blox system tracked a mean of 31.8 satellites (minimum = 26, maximum = 39) and the Trimble system tracked a mean of 30.0 satellites (minimum = 24, maximum = 35). The difference is due to the improved continuous signal tracking of Beidou satellites by the u-blox receiver (Fig. 3g-h). The positional dilution of precision (PDOP) is a measure of the strength of the receiver–satellite geometry. Lower PDOP values indicate a stronger geometry (i.e., satellites are well-distributed rather than clustered across the sky). The receivers experienced similar small excursions in PDOP (Fig. 3i-j), which is reflected as an increase in noise and poorer precision, particularly in the vertical component (for example, see the epochs at 0745 UTC for the Trimble solution, column 2). Overall, excellent PDOP values approaching 1 were observed for both u-blox and Trimble systems. A  $\text{PDOP} > 10$  indicates a poor receiver–satellite geometry (e.g., Teunissen and others, 2014).

The horizontal and vertical precisions of the two systems are nearly identical (Fig. 3). The horizontal root mean square ( $\text{RMS}_{2\text{D}}$ ) error is 2.4 mm for both the u-blox and Trimble GNSS stations (Table 4). The u-blox system also provided a marginal improvement in vertical precision in comparison to the Trimble system (u-blox:  $\sigma_u = 5.6$  mm vs. Trimble:  $\sigma_u = 5.9$  mm, Fig. 3). The corresponding 95% confidence ellipses are a 2D representation of the positional errors associated with the low-cost receiver (Fig. 4). Positioning errors are of a similar magnitude for u-blox and Trimble systems (Ub: length of the ellipse semi-major axis = 9.4 mm, Tr: 9.2 mm). The approximate north–south orientations of the ellipse semi-major axes are consistent with fewer positioning satellites traversing the southern sky at a high latitude site. This geometrical configuration, where satellite trajectories are less frequent in the southern sky, is depicted by the skyplots presented in Fig. 5.

High-precision (mm to cm-level) GNSS positions are achieved by carrier phase integer ambiguity resolution. If the number of complete carrier phase wavelengths between receiver and satellites is resolved as an integer value,

**Table 4.** The precision of u-blox and Trimble GNSS observations.  $\sigma_e$ ,  $\sigma_n$ , and  $\sigma_u$  denote the standard deviation of the easting, northing and vertical positions. For Experiment 2,  $\sigma_n$  is the standard deviation of the detrended northing positions (i.e., the mean downstream flow is removed). For Experiment 3 (dynamic observations), standard deviations  $\sigma_e$ ,  $\sigma_n$ , and  $\sigma_u$  are computed for 30-minute moving windows and presented as the mean for each time series. The 2D (horizontal) and 3D root mean square (RMS) errors are also computed for 30-minute moving windows and presented as the mean (Experiments 2 and 3). The mean position is taken as the reference value for each RMS error calculation.

		Receiver + antenna	$\sigma_e$ (mm)	$\sigma_n$ (mm)	$\sigma_u$ (mm)	RMS <sub>2D</sub> (mm)	RMS <sub>3D</sub> (mm)
<b>Experiment 1</b> (Stationary)	Ub	u-blox + patch	1.5	1.9	5.6	2.4	6.1
	Tr	Trimble R10	1.5	1.8	5.9	2.4	6.4
<b>Experiment 2</b> (Dynamic, medium baseline)	Ub1	u-blox + surveying	7.0	9.6	24.4	8.4	20.2
	Ub2	u-blox + patch	8.4	9.2	26.9	9.7	23.2
	Tr1	Trimble R10	6.5	8.5	26.6	8.3	22.0
<b>Experiment 2</b> (Dynamic, long baseline)	Ub1	u-blox + surveying	5.7	6.9	28.4	6.2	21.2
	Ub2	u-blox + patch	9.8	10.7	38.4	9.9	29.7
	Tr1	Trimble R10	5.3	7.5	37.4	6.5	22.4
<b>Experiment 3</b> (Dynamic, medium baseline)	Ub1	u-blox + surveying	4.3	5.7	17.0	7.1	18.4
	Ub2	u-blox + surveying	4.8	6.4	15.9	8.1	17.8
	Ub3	u-blox + patch	5.1	6.7	19.4	8.7	21.1
	Ub4	u-blox + patch	5.1	6.3	18.6	8.3	20.3
	Tr1	Trimble R10	4.6	6.0	16.7	7.6	18.3
	Tr2	Trimble R10	4.0	5.5	15.0	6.9	16.5

the solution is fixed. Float solutions, which inherently have poorer precision, are used when integer ambiguities are not resolved. The probability of correct integer estimation, also referred to as the integer ambiguity success rate, is 88.6% for u-blox and 91.4% for Trimble, suggesting a similar ambiguity resolution performance between the two receivers. Solutions were classified as fixed or floating according to a commonly used ambiguity ratio test within RTKLIB with a conservative ratio threshold of three (e.g., Teunissen, 2017, pg. 680). Since the traditional ratio test is not always robust (Teunissen and Verhagen, 2009; Verhagen and Teunissen, 2013), we also evaluate the positions by comparing the solutions to precise benchmark coordinates. With a threshold of  $\pm 5$  cm in the E/N/U directions, u-blox and Trimble systems achieved a 100.0% and 99.9% success rate, respectively, indicating a competitive performance between the two receivers. Therefore, in the following sections, we will assess the positioning performance based on solutions where ambiguities are assumed to have converged to their correct integer values. In other words, we will assess the positioning performance after convergence time for each solution.

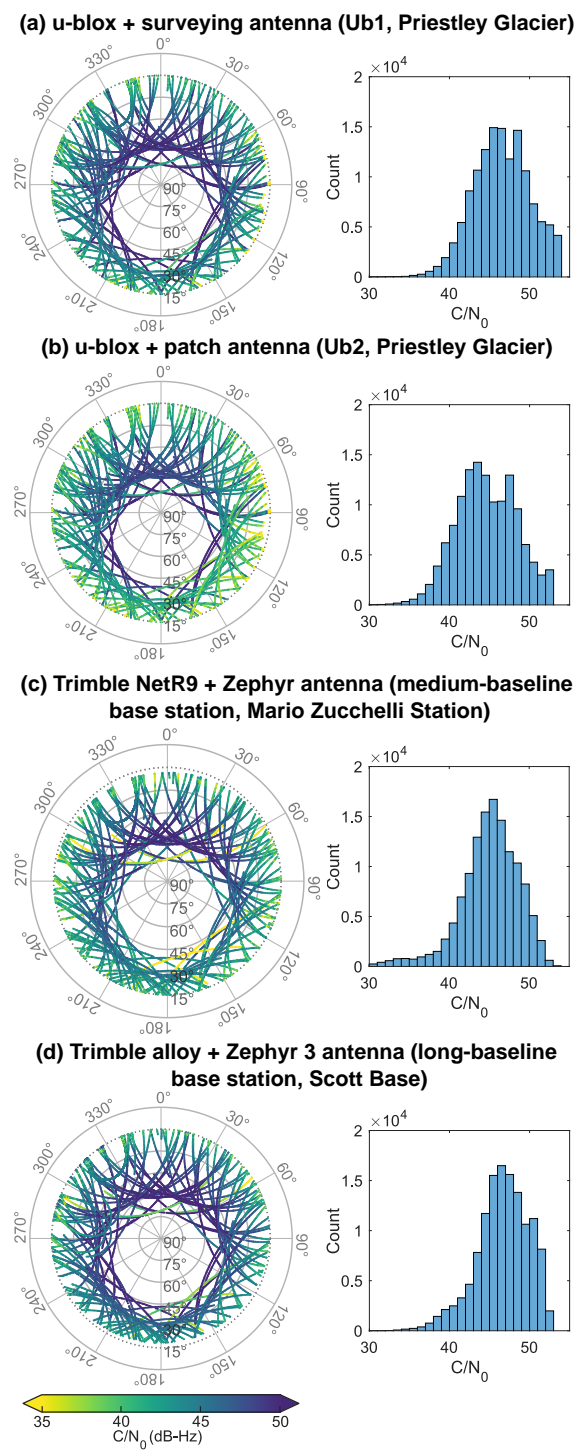


**Fig. 5.** Satellite skyplots with carrier-to-noise ( $C/N_0$ ) density ratios associated with each GNSS unit. Satellite trajectories in each skyplot are shown for 12 hours on 21 November, 2022 with an elevation cutoff of  $15^\circ$ . All constellations are included (GPS L1, GLONASS L1, Galileo E1, Beidou B1, QZSS L1). The  $0^\circ$  azimuth corresponds to geographic north.

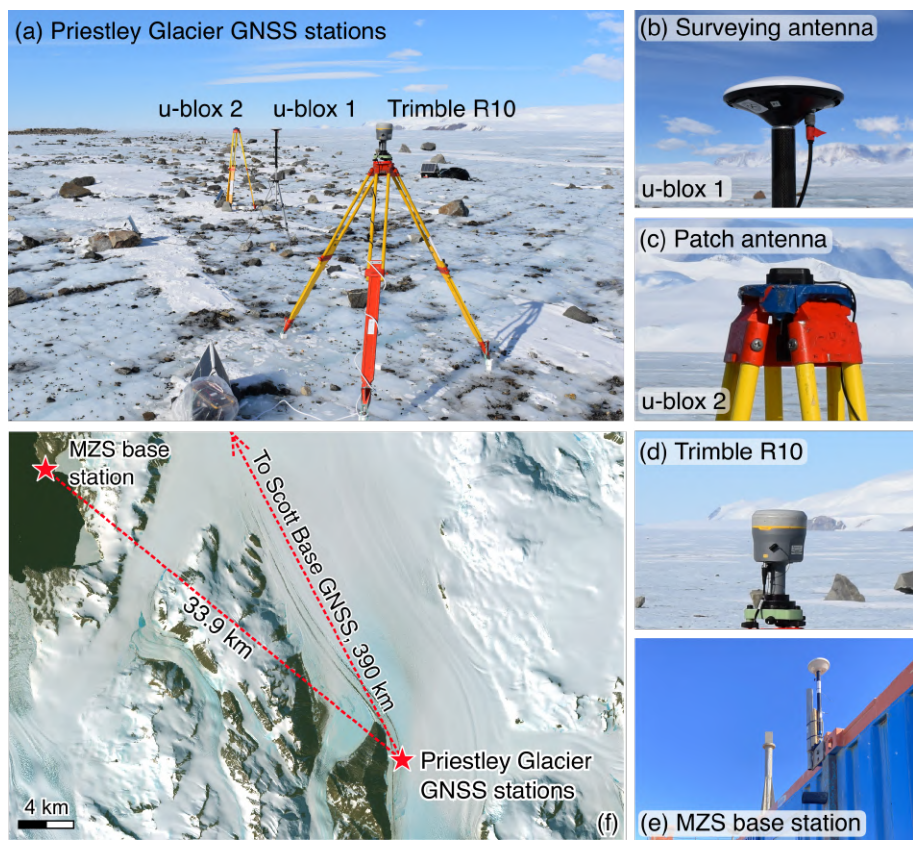


**Fig. 6.** Low-cost u-blox and survey-grade Trimble receivers and antennas installed on Priestley Glacier for 15 hours on 21 November, 2022 (Experiment 2). Panel (a) demonstrates the configuration of the roving receivers. Panels (b-d) show the antenna models compared in the experiment. Panel (e) demonstrates the set-up of the temporary base station installed at Mario Zucchelli Station (MZS). Panel (f) illustrates the configuration of the medium (33.9 km) and long (390 km) baselines in Experiment 2. The basemap in (f) is a Sentinel-2, 10 m true-colour image acquired on 18 December, 2022, courtesy of the European Space Agency.

## 248 4 EXPERIMENT 2: DYNAMIC, MEDIUM AND LONG-BASELINE 249 POSITIONING

250 This experiment evaluates the dynamic performance of the low-cost systems in a glaciated setting. Two u-blox (Ub1  
251 and Ub2) and one Trimble R10 (Tr1) GNSS station(s) were installed adjacent to each other on the floating left shear  
252 margin of Priestley Glacier (Fig. 6a). Station Ub1 was paired with a patch antenna (U-blox, 2022a) and Ub2 was  
253 paired with an alternative low-cost surveying antenna (GNSS OEM, 2023) (Fig. 6b and c) to assess whether low-cost  
254 antenna type affects positioning performance. The GNSS stations were aligned in a flow-oriented transect with a 5 m  
255 spacing. Antennas were installed 2 m above the ice surface with antenna centres positioned at the same elevation to  
256 ensure equivalent sky-view conditions. Positions were logged at a 1-second measurement interval for 15 hours during

257 the neap tide on 21 November, 2022. Maximum windspeeds of 12 knots were recorded during the experiment.

258 The dynamic positioning performance of the u-blox and Trimble systems is evaluated for medium (33.9 km) and  
259 long (390 km) baseline configurations. A temporary base station (Trimble NetR9 receiver + Zephyr model antenna)  
260 was installed on the roof of a shipping container GNSS laboratory at Mario Zucchelli Station to support the medium  
261 baseline (33.9 km) test. This receiver tracked GPS, GLONASS, Galileo, Beidou and QZSS satellite signals at 1 Hz  
262 (Fig. 6e). Existing reference stations in the Terra Nova Bay region do not record all available constellations and  
263 frequencies, and thus were unsuitable for this objective (Mario Zucchelli and Jang Bogo Station reference stations:  
264 both GPS and GLONASS only). The base station used for the long baseline test is the International GNSS Service  
265 (IGS) ground station (SCTB) established near Scott Base, 390 km southeast of Priestley Glacier (Johnston and  
266 others, 2017; LINZ, 2023). This receiver tracks GPS, GLONASS, Galileo, Beidou and QZSS satellite signals at a 10  
267 second measurement interval.

#### 268 4.1 Medium-baseline positioning performance

269 Low-cost stations Ub1 (surveying antenna) and Ub2 (patch antenna) provided millimetre-level precision (Fig. 7).  
270 Horizontal RMS<sub>2D</sub> errors were 8.4 mm and 9.7 mm for Ub1 and Ub2, respectively. The u-blox receivers were  
271 competitive with the Trimble system (RMS<sub>2D</sub> error: 8.3 mm), irrespective of choice of low-cost antenna (Table 4,  
272 Fig. 7). The almost identical performance of the low-cost and survey grade instruments is also shown by similarities  
273 in the derived ice velocity estimates. Based on only 12 hours of observations, ice velocities of  $99.9 \pm 0.4 \text{ ma}^{-1}$  (Ub1),  
274  $103.2 \pm 0.4 \text{ ma}^{-1}$  (Ub2),  $98.9 \pm 0.3 \text{ ma}^{-1}$  (Tr1) are estimated. No tidal vertical oscillation is observed because positions  
275 were recorded during the neap tide at a site near a glacier margin.

276 The vertical positioning error is approximately 3 to 4 times the horizontal error for both u-blox and Trimble  
277 observations from Priestley Glacier (Table 4, Fig. 7). The ratio between the vertical and horizontal error magnitude  
278 is closer to 2 at lower latitude sites (e.g., Yong and others, 2021; Tidey and Odolinski, 2023), due to a more favourable  
279 receiver–satellite geometry. While the total number of tracked satellites at the Priestley Glacier site is relatively high  
280 ( $n = 30$  to 32) and comparable to a mid-latitude site, the elevation angles of the satellites are lower at higher latitudes  
281 (Fig. 5). The geometry leads to a weaker vertical dilution of precision (VDOP), while the horizontal dilution of  
282 precision (HDOP) remains close to 1. A similar effect was also observed for the short baseline, stationary scenario  
283 (Experiment 1).

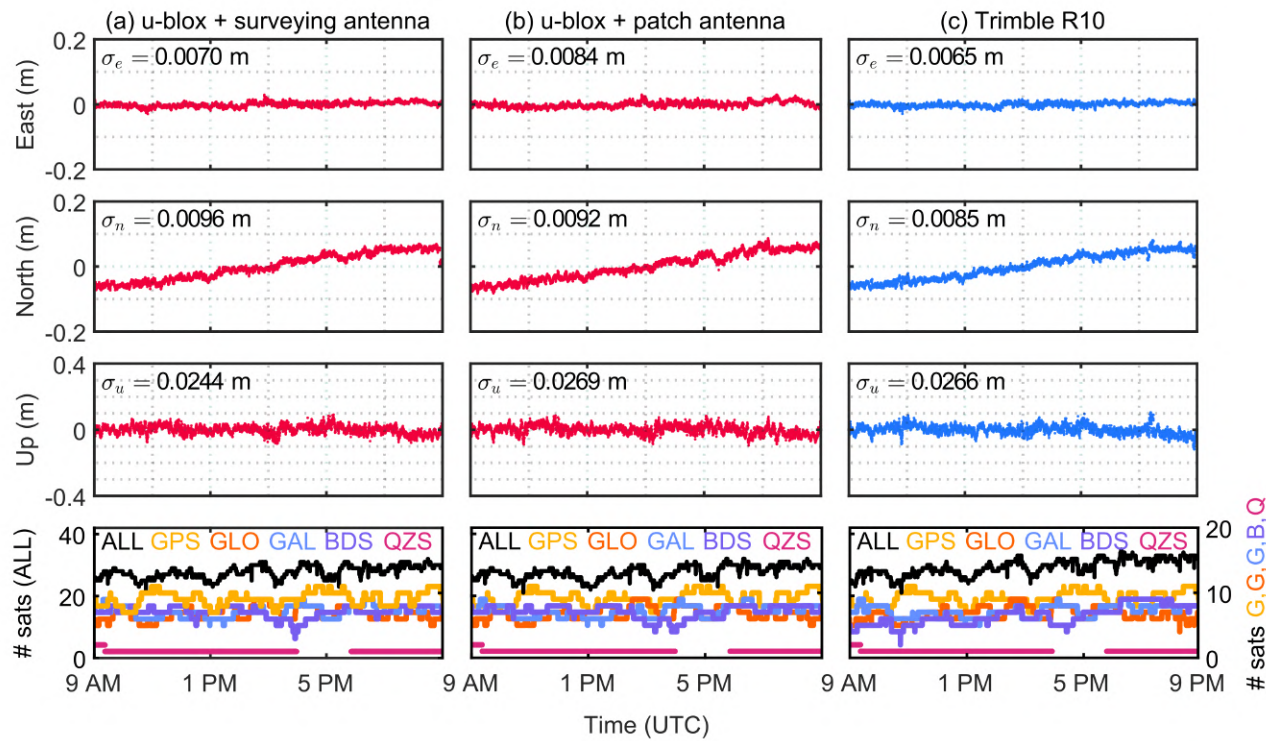


**Fig. 7.** Medium-baseline, dynamic positions recorded with u-blox and Trimble GNSS stations installed on Priestley Glacier for a 12 hour observation period on 21 November, 2022 (Experiment 2). East and north components of position correspond to the horizontal axes of the Antarctic Polar Stereographic coordinate system (EPSG:3031), with the mean position removed. Eastings and northings also correspond to local across-flow and along-flow directions, respectively (Fig. 1c). The baseline between the NetR9 base station and the on-glacier receivers is 33.9 km.  $\sigma_e$  and  $\sigma_u$  are standard deviations and  $\sigma_n$  is the standard deviation of the detrended northing component of position (i.e., displacement downstream).  $n = 4320$  epochs are included in each time series. Note the change in  $y$ -axis limits from  $\pm 0.2$  m for the horizontal components to  $\pm 0.4$  m for the vertical component.

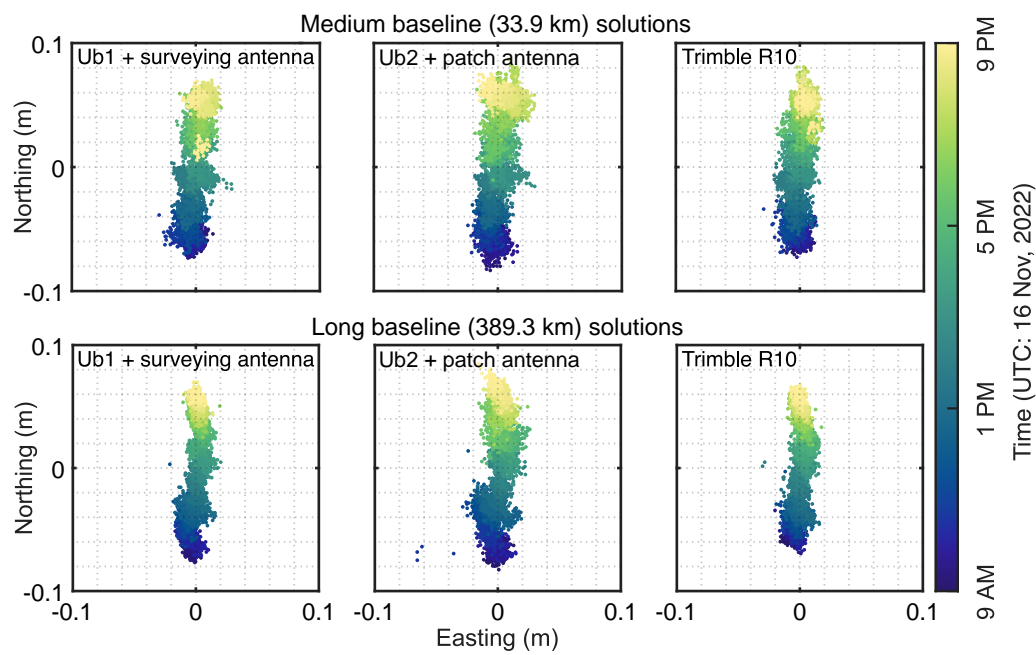


**Fig. 8.** Horizontal trajectories of the u-blox and Trimble GNSS stations installed alongside each other on Priestley Glacier for 12 hours on 21 November, 2022 (Experiment 2).  $n = 4320$  epochs are included in each solution.

#### 284 4.2 Long-baseline positioning performance

285 All GNSS stations (Ub1, Ub2, Tr1) were capable of millimetre-level horizontal precision in a long baseline (390 km)  
 286 configuration (Figs. 8 and 9). Low-cost station Ub1 paired with the surveying antenna was competitive with the  
 287 Trimble system (RMS horizontal errors were Ub1 = 6.2 mm and Tr1 = 6.5 mm). Of the three stations, the horizontal  
 288 and vertical positions acquired with the patch antenna were more susceptible to cycle slips and measurement noise  
 289 (Fig. 9). All long baseline solutions presented here use three satellite constellations only (GPS+GLONASS+Galileo).  
 290 Further improvements in long-baseline positioning performance are expected with the inclusion of Beidou and QZSS  
 291 satellites (e.g., Odolinski and others, 2014; Odolinski and Teunissen, 2017a).

292 Vertical positioning errors for all stations increased by approximately 30% in comparison to the medium baseline  
 293 errors (Table 4). Conversely, the long-baseline configuration did not increase horizontal positioning errors despite  
 294 the order of magnitude increase in baseline length. With all other error sources held equal, error magnitudes increase  
 295 with increasing distance between base station and rover. We attribute the better-than-expected long-baseline results  
 296 to the superior antenna hardware and placement of the Scott Base IGS network station. The temporary base station  
 297 installed at Mario Zucchelli Station to support the medium baseline test was installed in a high-wind zone on top of  
 298 a shipping container and paired with an early model, lightweight Zephyr antenna of slightly inferior quality to the

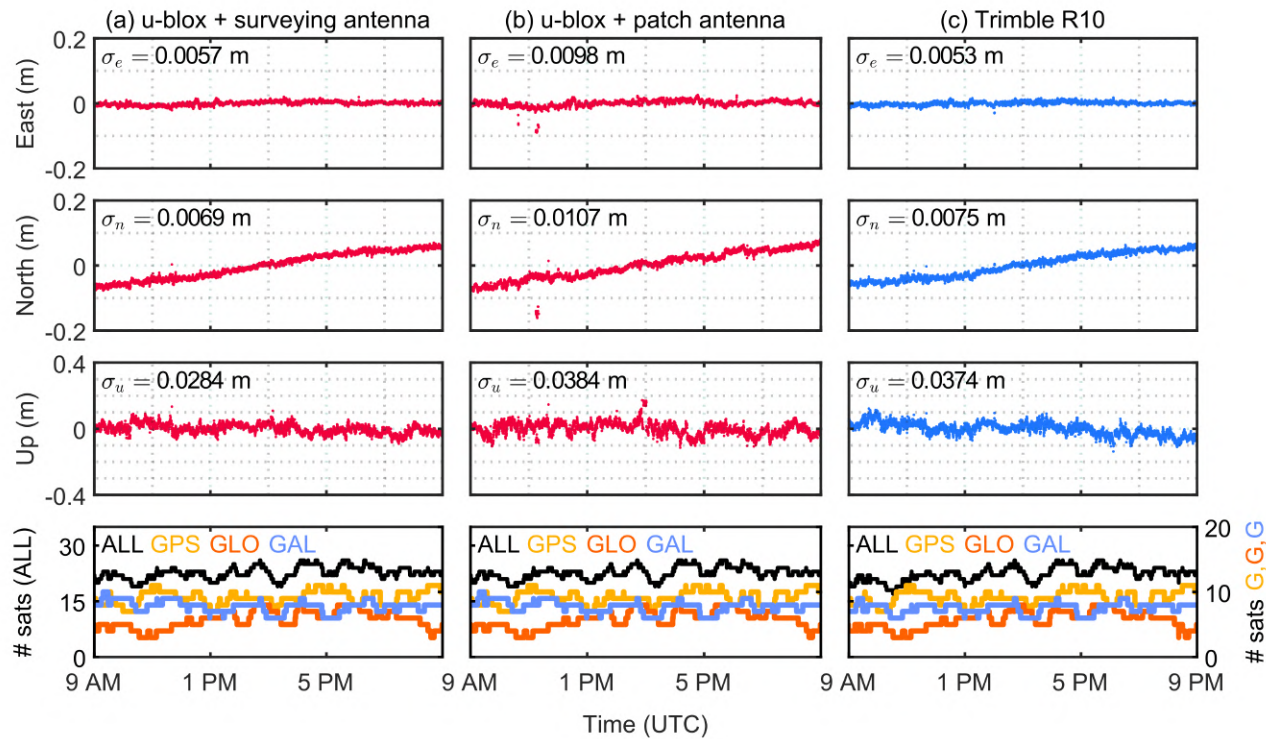


**Fig. 9.** Long-baseline, dynamic positions recorded with u-blox and Trimble GNSS stations installed on Priestley Glacier, for a 12-hour observation period on 21 November, 2022 (Experiment 2). The baseline between the Scott Base reference station and the on-glacier receivers is 390 km.  $\sigma_e$  and  $\sigma_u$  are standard deviations and  $\sigma_n$  is the standard deviation of the detrended northing component of position (displacement downstream).  $n = 4320$  epochs from a 12-hour observation period are included in each time series. Note the change in  $y$ -axis limits from  $\pm 0.2$  m for the horizontal components to  $\pm 0.4$  m for the vertical component.

299 IGS station antenna (Fig. 6e). The IGS station is equipped with a Zephyr 3 geodetic antenna, designed to minimise  
300 multipath via a large resistive ground plane. The difference in antenna hardware quality is shown by the distribution  
301 of the carrier-to-noise ( $C/N_0$ ) density ratios (a measure of signal strength, Fig. 5), where overall, observations from  
302 the Scott Base IGS station have higher  $C/N_0$  values than the Mario Zucchelli base station.

### 303 4.3 Multi-GNSS versus GPS positioning performance

304 This test compares multi-GNSS solutions (GPS, GLO, GAL, BDS, QZS) to single (GPS) and dual-GNSS (GPS  
305 and GLONASS) solutions from the medium-baseline (33.9 km) experiment conducted on Priestley Glacier. As  
306 expected, the five-constellation positioning solution yields smaller errors than the single (GPS) and dual-GNSS (GPS  
307 + GLONASS) solutions for both u-blox and Trimble systems (Fig. 10). Each multi-GNSS positioning solution  
308 includes at least twice as many tracked satellites in comparison to the single and dual-constellation solutions, leading  
309 to less measurement noise and a reduced frequency of undetected cycle slips that are characteristic of the single and  
310 dual-constellation solutions.

311 The low-cost u-blox system only achieves competitive performance to the Trimble system when three or more  
312 constellations are tracked. The Trimble system, however, provided centimetre-level precision for single (GPS) and  
313 dual (GPS + GLONASS) solutions, at epochs when the u-blox system experienced high signal noise and cycle  
314 slips (e.g., Fig. 10, epochs at 1000 UTC). One key advantage of the higher-cost Trimble system is therefore the  
315 ability to achieve precise positions and a stable time series unaffected by cycle slips when only GPS and GLONASS  
316 observations are available. We recommend that u-blox rover and base station pairs are configured to track at least  
317 GPS, GLONASS and Galileo satellites, at two or more frequencies, for successful low-cost GNSS positioning. To  
318 summarise, the dual-GNSS system (GPS+GLONASS) provided millimetre to centimetre-level precision when using  
319 a survey-grade receiver and antenna (Fig. 10), but may not suffice when using a low-cost GNSS system at this site.

### 320 4.4 Low-cost antenna performance

321 The medium and long baseline experiments also evaluate the potential impact of different low-cost antenna types on  
322 the precision of the positioning results. For the long baseline, horizontal precision improved when the u-blox receiver  
323 Ub1 was paired with a multiband surveying antenna instead of a multiband patch antenna (RMS<sub>2D</sub> error for Ub1:  
324 6.2 mm vs. Ub2: 9.9 mm). Similarly, the surveying antenna also improved the vertical precision for both medium  
325 and long baseline solutions (Table 4). Antenna type had no impact on horizontal error magnitudes in the medium  
326 baseline test.

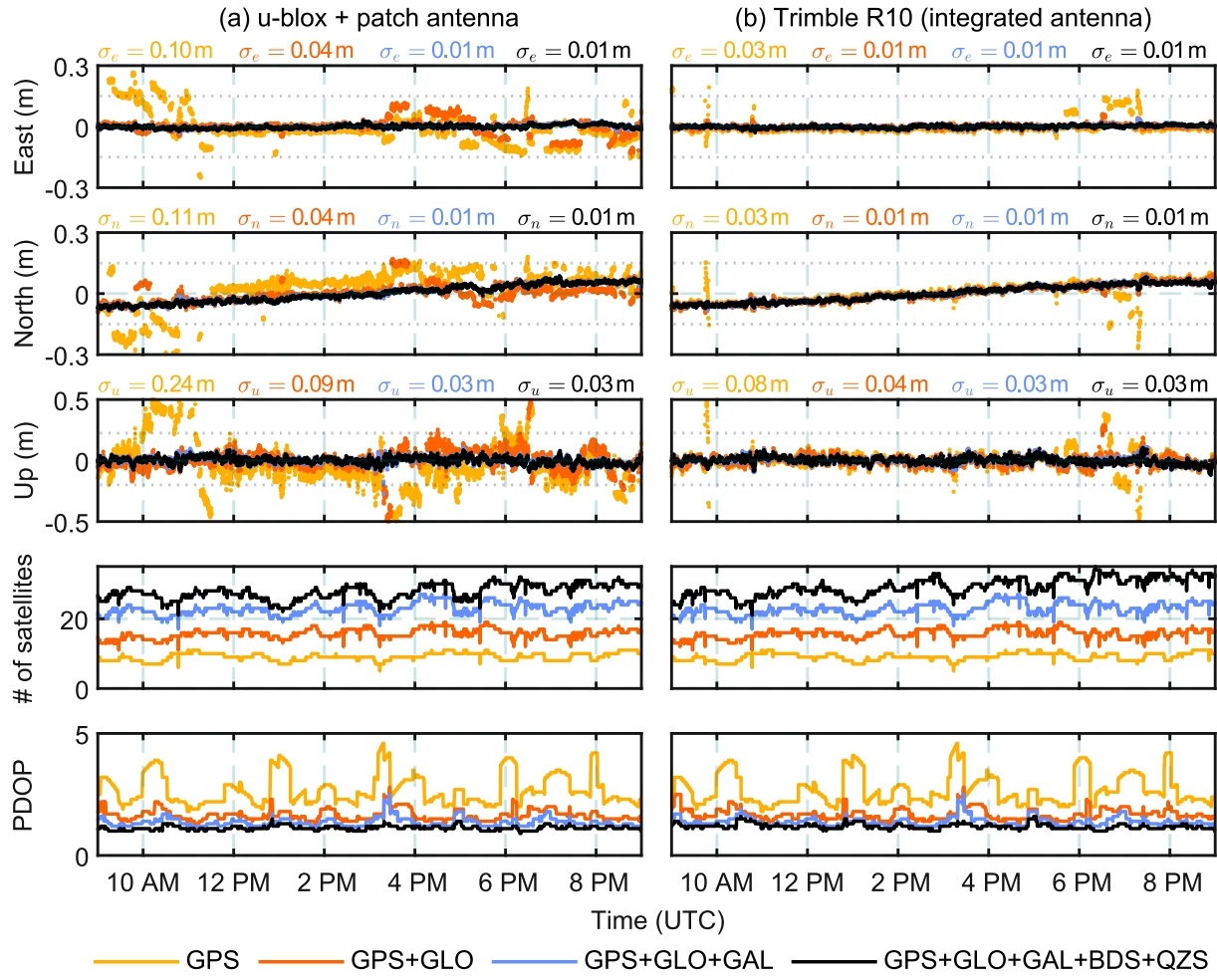


**Fig. 10.** East (across-flow), north (along-flow) and vertical (up) positioning solutions for two Priestley Glacier GNSS stations with the inclusion of additional satellite constellations. Each time series includes  $n = 4320$  epochs (10 s sample interval) collected over a 12-hour observation period on 21 November, 2022. The number of satellites is computed for an elevation cutoff angle of  $15^\circ$ . U-blox (a) and Trimble R10 (b) GNSS stations were installed as part of Experiment 2 (Fig. 6). Note the change in  $y$ -axis limits from  $\pm 0.3$  m for the horizontal components to  $\pm 0.5$  m for the vertical component.

327 The long baseline positions obtained with a patch antenna have larger error magnitudes because the simplified  
328 antenna hardware is more susceptible to signal noise (Fig. 5). Patch antennas do not contain internal shielding to  
329 mitigate multipath effects and cycle slips are also more frequent due to the antenna receiving a weaker, noisier signal  
330 (Fig. 9b). Raw signals received by the u-blox + patch antenna system have lower  $C/N_0$  values overall, particularly  
331 for lower elevation satellites ( $<30^\circ$ ) (Fig. 5a-c). In other settings, low-cost patch antennas are also shown to have a  
332 lesser ability to suppress multipath interference and signal noise (Odolinski and Teunissen, 2017a; Romero-Andrade  
333 and others, 2021; Paziewski, 2022; Manzini and others, 2022).

## 334 5 EXPERIMENT 3: MULTI-DAY GNSS RECORDS OF ICE MOTION

335 Low-cost and survey-grade GNSS performance is evaluated in a realistic glacier monitoring scenario: observing tide-  
336 modulated ice flexure across the floating shear margin of Priestley Glacier. Multi-day records of glacier motion were  
337 observed at six GNSS stations (4 u-blox, 2 Trimble R10s) arranged in across- and along-flow transects (Fig. 1c,  
338 Table 2). We present six GNSS time series of tidally-modulated across- and along-flow ice displacement and velocity  
339 with estimated positioning errors. In this experiment, the amplitudes of the E/N/U position time series for each  
340 station will vary due to the different receiver locations with respect to the glacier margin, while the timing of high  
341 and low tide peaks should be synchronised.

342 Vertical ice motion at a predominantly solar diurnal tidal frequency is observed at all GNSS sites (Fig. 11).  
343 Focusing on the low-cost configurations, stations Ub4 (600 m from the margin) and Ub3 (800 m from the margin),  
344 detected clear diurnal tidal oscillations with amplitudes less than 1 and 2 cm, respectively (Fig. 11a), synchronised  
345 with the timing of the CATS2008 tide prediction (Padman and others, 2002; Howard and others, 2019). Vertical  
346 positions recorded by the three GNSS stations in the along-flow transect (Fig. 11b) have very similar signal amplitudes  
347 and error magnitudes, irrespective of receiver or antenna type. Similar uncertainties are achieved in all of the GNSS  
348 configurations reported here (Fig. 11, Table 4). For example, the average of the moving standard deviation  $\sigma_u$ , a  
349 measure of observation noise associated with vertical positioning, is 4.3 cm (Ub3) and 4.0 cm (Ub4) for the u-blox  
350 + patch antenna configurations, and 3.8 cm (Ub1) and 3.7 cm (Ub2) when standard surveying antennas are used.  
351 Three explanations for marginally smaller vertical errors derived from stations Ub1 and Ub2 are firstly the more  
352 advantageous satellite–receiver geometry – the receivers were installed a greater distance from Black Ridge and have  
353 an unobstructed skyview (Fig. 1c). Ub1 and Ub2 were also able to track an additional 1 to 2 satellites at each epoch  
354 and were paired with low-cost surveying antennas rather than patch antennas.

355 Tidally-modulated along- and across-flow ice displacement is observed at all GNSS stations (Fig. 12). All u-blox

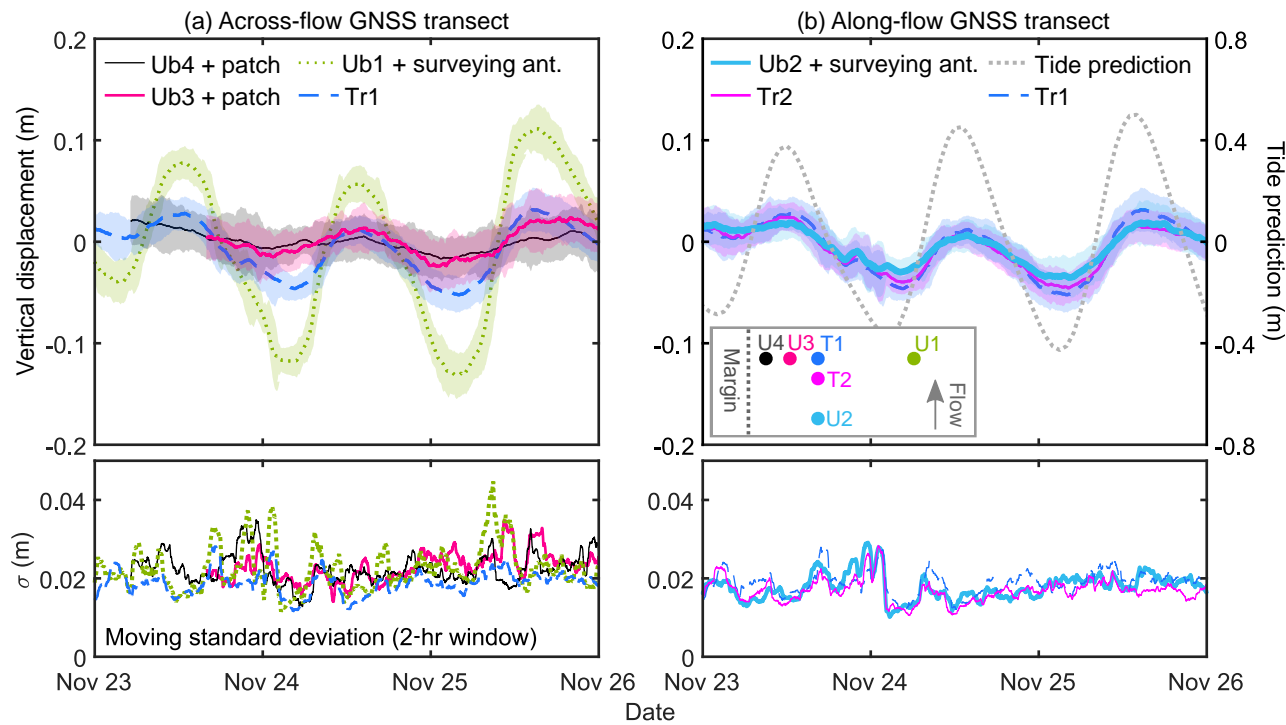


**Fig. 11.** The tide-modulated vertical displacement of four u-blox and two Trimble GNSS stations on Priestley Glacier. Panel (a) includes the stations installed in an across-flow transect. Panel (b) includes the stations installed in an along-flow transect, and a tide prediction from the CATS2008 model (Padman and others, 2002; Howard and others, 2019). Shaded error bounds show the moving standard deviation (two-hourly window) of the vertical position time series. These GNSS stations are expected to exhibit vertical oscillations with varying amplitudes due to their different locations with respect to the glacier margin and grounding zone. Predicted tidal amplitudes and GNSS-observed amplitudes differ because the Priestley Glacier field site is not freely-floating in hydrostatic equilibrium. GNSS station locations are mapped in Fig. 1c.

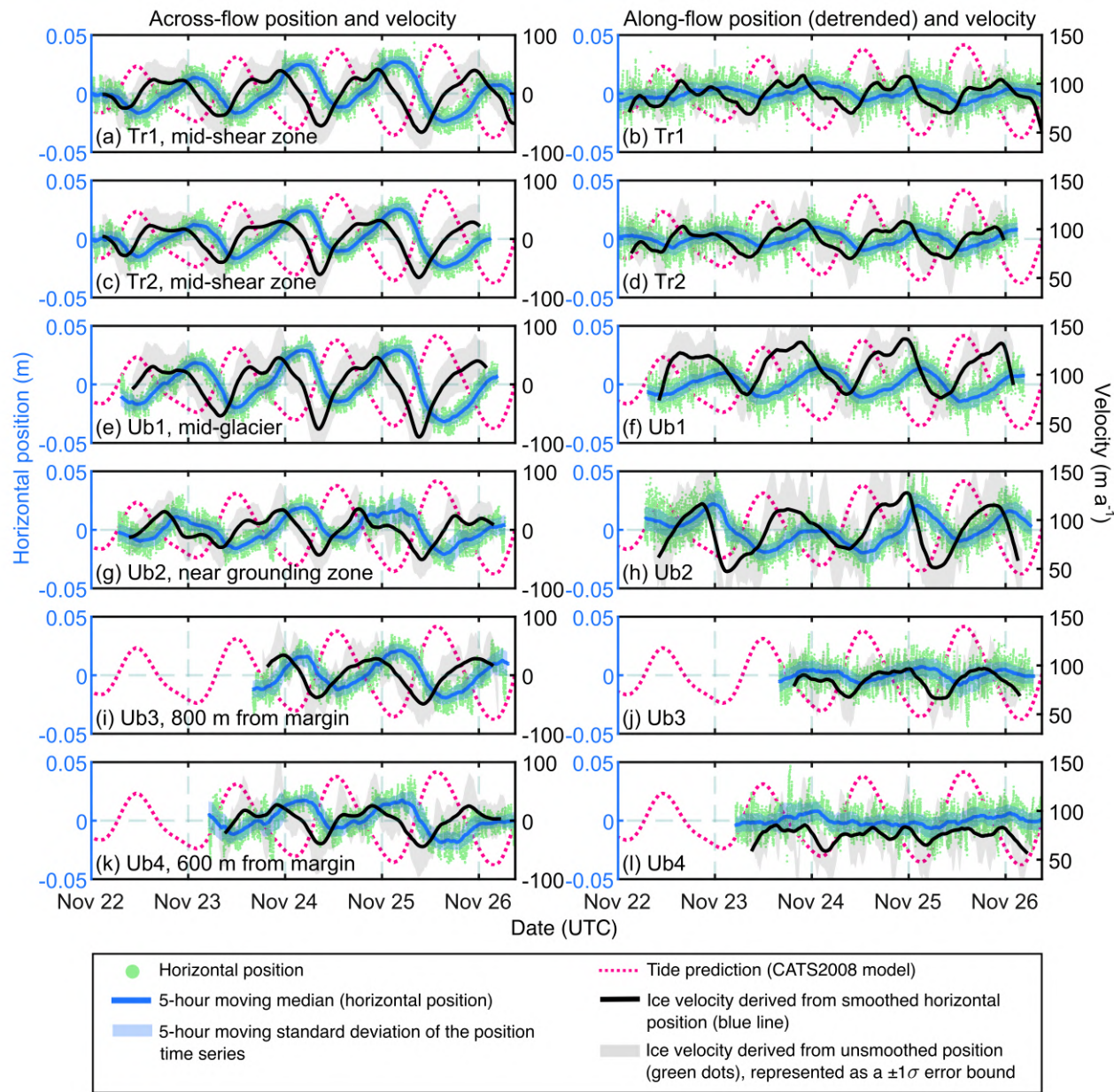


**Fig. 12.** Across and along-flow ice displacement and velocity at each Priestley Glacier GNSS station. GNSS positions (green dots) are smoothed with a five-hour moving median filter (dark blue line). Shaded blue error bounds represent  $\pm 1\sigma$  in horizontal position over a five-hour sliding window. In column 1, across-flow displacement in the negative (positive) direction indicates motion toward (away from) the glacier margin. In column 2, the along-flow displacement is presented with the mean linear flow removed. Along-flow displacement in the positive direction indicates an increased downstream flow rate. The ice velocity (black line) is a linear least-squares fit between the smoothed displacement (blue line) and time. The grey error band denotes the velocity computed from unsmoothed positions (green dots), presented as a  $\pm 1\sigma$  error band. The tide prediction is from the CATS2008 model (Padman and others, 2002; Howard and others, 2019). Neap tide occurred on the 20 November, 2022.

and Trimble stations operated with a precision that allowed the detection of velocity variability at a diurnal frequency (Fig. 12). In the along-flow direction, ice velocity increases during the falling tide, and slows during the rising tide, with one velocity maximum observed per diurnal tide cycle. In the across-flow direction, the observed transverse displacement of ice (towards and away from the margin) is associated with elastic bending. On the rising tide, ice is displaced toward the margin and on the falling tide ice is displaced toward the glacier centre (Fig. 12). The amplitude of these oscillations ranges from ±1.5 cm (Ub4, nearest the glacier margin) to ±3 cm (Ub1, nearest the glacier centre).

### 5.1 Sources of positioning error

In this section, we consider the causes of positioning errors at the Priestley Glacier field site. Variability in positioning noise is shown by the moving standard deviation computed for each position time series (Fig. 11b). Peaks and trends in the moving standard deviations are synchronised between all six of the GNSS stations, despite their different locations across the glacier shear margin. This consistency across GNSS stations indicates that variability in positioning noise is not predominately due to site specific multipath interference effects or differences in hardware (low-cost versus survey-grade receivers, or standard versus patch antennas). Instead, the number of tracked satellites, or the similarities in ionospheric and tropospheric conditions, may determine the magnitude of positioning errors at the Priestley Glacier site.

Time-varying satellite geometry and atmospheric effects are demonstrated using the longest duration position time series from station Tr1 (Trimble R10, 10-day duration, Fig. 13). Short-term increases in positioning noise coincide with rapid decreases in the number of tracked positioning satellites (e.g., the epochs at 0800 hours on November 19 in Fig. 13c). The HDOP and PDOP, however, remain steady over the ten-day measurement period due the high number of positioning satellites tracked at all epochs (Fig. 13f). A second source of error, the prevailing ionospheric conditions (indicated by the K<sub>p</sub> index), has no apparent association with observed positioning noise (Fig. 13e). Similarly, large variations in the slant ionospheric delay, defined as the estimated delay as the GNSS signal passes through the ionosphere, have very little association with positioning error magnitudes. This result indicates that the ionospheric delay modelling strategy (Table 3) correctly estimates the ionospheric delays. Priestley Glacier GNSS datasets were collected during a period of low to medium ionospheric disturbance (K<sub>p</sub> index ≤ 4). A longer time series encompassing a wider range of geomagnetic disturbances is required to further investigate these effects. Indeed, low-cost GNSS hardware with poorer quality code and carrier phase measurements may be more susceptible to degraded positioning performance during periods of strong ionospheric activity.

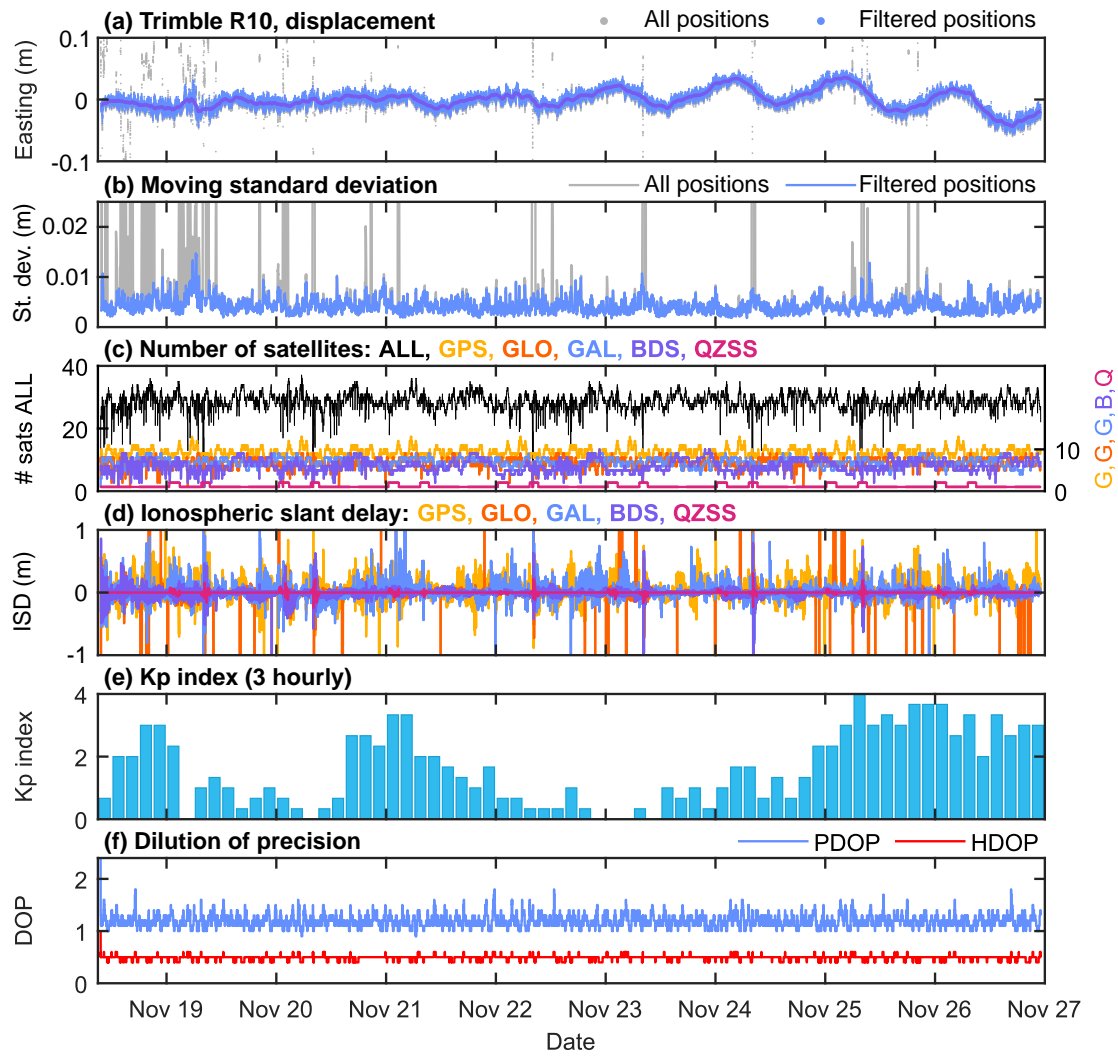


**Fig. 13.** The association between positioning noise, satellite–receiver geometry and ionospheric conditions at station Tr1. Panel (a) shows the easting component of position. Filtered position time series have outliers removed as described in Section 2.2. Panel (b) shows the corresponding moving standard deviation, computed for 1-hourly windows (360 epochs). Panel (c) shows the number of satellites tracked at each epoch. Panels (d) and (e) show the slant ionospheric delay and the Kp index (NOAA, 2023), a measure of global ionospheric disturbance. Panel (f) shows the variability in the horizontal dilution of position (HDOP) and positional 3D dilution of precision (PDOP). In this analysis, only the easting component of horizontal position is presented for brevity. Similar conclusions are drawn from time series of the northing and vertical components of position.

## 385 6 DISCUSSION

386 GNSS positioning performance at high latitude sites may be affected by relatively low satellite elevations, which result  
387 in weaker receiver–satellite geometries and longer signal paths through the ionosphere. Nonetheless, the positioning  
388 performance of u-blox GNSS stations at our high-latitude glacier site is similar to performance evaluations of the  
389 same equipment at mid-latitude sites. For example, kinematic positioning evaluations of u-blox receivers have  
390 reported horizontal precision of  $\sigma_e$  and  $\sigma_n = 10$  mm (Odolinski and Teunissen, 2020) (RTK, long baseline: 112  
391 km) and  $\sigma_e = 8$  and  $\sigma_n = 10$  mm (Tidey and Odolinski, 2023) (RTK, medium baseline: 27 km). In the present  
392 experiments, equivalent data processing approaches applied to low-cost and survey-grade observations with three or  
393 more constellations resulted in comparable RMS errors for each baseline length (Table 4). The high-cost, survey-grade  
394 system offered no performance advantages. At longer baselines, pairing the low-cost receiver with a ground-plane  
395 surveying antenna (rather than a patch antenna) resulted in a small improvement in precision.

396 The present work focuses on single-baseline kinematic positioning (a relative positioning method) because it can  
397 provide the millimetre- to centimetre-level precision required for glaciological applications. Error magnitudes are a  
398 function of baseline length, with millimetre-level precision anticipated for short baselines ( $<20$  km). However, the  
399 common notion that a base station must be located within a few tens of kilometres is not necessarily a requirement,  
400 particularly for dual-frequency, multi-GNSS observations. Centimetre-level precision is feasible over long baselines  
401  $>100$  km (Schüler, 2006; Odolinski and Teunissen, 2020), and indeed, the present work achieved centimetre-level  
402 precision for both low-cost and survey-grade systems with a 390 km baseline (Fig. 9).

403 Successful positioning with the low-cost u-blox system is possible with both single-baseline kinematic positioning,  
404 and single-receiver PPP (Zumberge and others, 1997). While we use kinematic positioning due to its inherently  
405 smaller error magnitudes at short to medium baselines, remote field settings may necessitate the application of PPP  
406 techniques. To illustrate the performance of PPP with low-cost hardware, we generate example solutions using the  
407 online CSRS-PPP service (GPS+GLONASS only) and RTKLIB kinematic-PPP (GPS + GLONASS + Galileo) (see  
408 Supplementary Material). The choice of low-cost rather than survey-grade hardware did not compromise positioning  
409 performance for glaciological applications when using PPP.

### 410 6.1 Set-up of low-cost systems for successful precise positioning

411 The u-blox ZED-F9P receivers used here have the capability to track multi-GNSS dual-frequency signals (e.g., GPS  
412 and GLONASS: L1 and L2, Galileo: E1 and E5b). Dual-frequency observations enable medium and long-baseline  
413 positioning with low-cost systems (Odolinski and Teunissen, 2020). The GNSS signal is delayed as it travels through

the ionosphere, and this effect is amplified as baseline length increases and satellite elevation decreases, leading to errors on the order of tens of metres (Odijk and Wanninger, 2017). Estimation of the ionospheric delay is therefore necessary for medium and long baselines, but can be neglected for a shorter baselines, in which case the delays are approximately equal. Dual-frequency data is used to estimate slant ionospheric delays, leading to more precise estimates and improved ambiguity resolution performance (Odolinski and Teunissen, 2020). In the present work, centimetre-level precision over a long baseline (390 km) is achieved in this way. Single-frequency low-cost modules will not achieve comparable results. Multi-GNSS solutions (i.e., GPS + GLONASS + Galileo + Beidou + QZSS) provide an improved satellite geometry and redundancy in observations, leading to improvements in precision (e.g., Odolinski and others, 2015a; Paziewski and Wielgosz, 2017; Xue and others, 2021).

Single-constellation and dual-constellation solutions are widely used for GNSS positioning in Antarctica, particularly when employing PPP services such as the CSRS-PPP service (Banville and others, 2021), or when applying corrections from permanent long-term reference stations for kinematic positioning. In the latter case, existing GNSS reference stations in Antarctica are often configured to receive GPS and GLONASS signals only. For example, the nearby Mario Zucchelli and Jang Bogo Station reference GNSS stations in Terra Nova Bay both recorded GPS and GLONASS signals only during our field campaign. Installation of a temporary base station on stationary ground to track additional constellations may be beneficial for low-cost kinematic positioning if millimetre- to centimetre-level precision is required. The multi-GNSS solutions presented here outperformed the single or dual-constellation solutions for both low-cost and survey-grade receivers (Fig. 10).

The precision and accuracy of GNSS positions can be improved by pairing the low-cost receivers with survey-grade or geodetic antennas (e.g., Odolinski and Teunissen, 2017a; Paziewski, 2022; Romero-Andrade and others, 2021). Performance improvements associated with the use of geodetic or survey-grade antennas are well established and we do not evaluate this further here. Instead, we compared the performance of low-cost patch antennas and low-cost standard surveying antennas to meet the objective of using a purely low-cost system. In cases where sub-centimetre precision is required, or when working with long baselines exceeding 100 km, using a low-cost surveying antenna rather than a patch antenna may lead to improved precision (e.g., Table 4). In the long baseline (390 km) test (Experiment 2), we observed a 30% reduction in the 3D RMS error when using a low-cost surveying antenna instead of a patch antenna.

## 441 6.2 Applications and advantages of low-cost positioning in Antarctica

442 The low-cost positioning systems installed on Priestley Glacier consumed approximately half as much power as  
443 the survey-grade systems (Table 2). Power usage depends on the choice of receiver, data logger, and antenna  
444 hardware (amplified surveying multiband antenna models consume more power than patch antenna models), and  
445 the observation sampling frequency. Low-cost positioning systems used in the present work logged all available  
446 constellations at 1 Hz while supported by a pair of small 12 V solar panels (28 cm × 28 cm) and a single 18 A h  
447 SLA battery. The reduced power consumption of the low-cost system is a key advantage because the weight and  
448 bulkiness of an overwinter power system (battery bank + solar panels) is a burden for logistical resourcing. At  
449 present, continuous GNSS records of Antarctic ice dynamics are biased toward the summer months, with data gaps  
450 arising from the challenge of maintaining steady power supply during the polar winter (e.g., Jones and others, 2016;  
451 Greene and others, 2020; Klein and others, 2020). Low-cost GNSS stations, such as the dual-frequency u-blox units  
452 tested here, are a step toward continuous, year-round monitoring in remote environments where power requirements  
453 are logistically challenging.

454 Installation of a temporary low-cost base station to support a field campaign is possible without significant cost  
455 barriers. Where centimetre-level rather than decimetre-level precision is required, a low-cost, single-baseline solution  
456 may yield positions with better precision and accuracy than a PPP solution (Figs. S1 and S2). With dual-frequency  
457 receivers and multi-GNSS configurations such as the five-system (GPS+GLO+GAL+BDS+QZS) configuration used  
458 in the present work, medium- to long-baseline kinematic positioning (>300 km) is feasible (Experiment 2) and may  
459 provide improved precision and accuracy over PPP (Fig. S2). Long-baseline positioning solutions can also provide  
460 redundancy and quality control when relying on PPP solutions.

461 The precision of the positioning system determines the smallest measurable ice displacement or change in velocity.  
462 The low-cost GNSS units tested on Priestley Glacier operated with centimetre-level horizontal and vertical precision,  
463 suitable for a range of glaciological applications. Minimum horizontal and vertical tidal oscillations detected by the  
464 low-cost systems were ~1 cm and ~1.5 cm, respectively (Figs. 11 and 12). The precision of the low-cost units is  
465 suitable for the observation of tide-modulated velocity gradients within a single week-long field campaign, with no  
466 return to the site required. Nearer to the glacier margin, where ice displacement approaches zero, measurement noise  
467 begins to exceed the amplitude of displacement, although the mean position is well defined and tide signals are still  
468 detected. Low-cost GNSS units similar to the set-ups evaluated here are also suitable for densifying existing GNSS  
469 monitoring networks or reference stations. For single-season, temporary occupations of field sites, the significantly  
470 lower cost combined with lesser power consumption motivates the deployment of additional GNSS stations for

471 improved spatial coverage and repeatability for studies of ice kinematics and mechanics.

## 472 7 CONCLUSIONS

473 Low-cost, mass-market dual-frequency GNSS receivers are capable of precise and reliable positioning at high-latitude,  
474 glaciated sites, with errors comparable to high-cost systems. Horizontal and vertical positions from co-located u-blox  
475 ZED-F9P GNSS receivers (<\$300 USD) and survey-grade Trimble R10 receivers (>\$10,000 USD) were compared  
476 under stationary and dynamic conditions in Terra Nova Bay, Antarctica. RMS horizontal errors (Table 4) indicate  
477 almost identical performance for short baselines (u-blox + patch antenna: 2 mm, Trimble: 2 mm), medium baselines  
478 (u-blox + surveying antenna: 8 mm, Trimble: 8 mm) and long baselines (u-blox + surveying antenna: 6 mm,  
479 Trimble: 7 mm). A low-cost ground-plane surveying antenna provides a slight advantage over a patch antenna at  
480 longer baseline lengths.

481 Four low-cost GNSS stations and two survey-grade stations were installed on Priestley Glacier to evaluate the  
482 performance and reliability of each system in a challenging kinematic setting characterised by centimetre-level ice  
483 displacements. The efficacy of low-cost GNSS depends on the magnitude of the observation noise, relative to the  
484 signal of interest. Multi-day time series of 3D ice motion show that the low-cost systems operated with a level of  
485 precision useful for measuring tide-modulated velocity variability at semidiurnal and diurnal frequencies, at a field  
486 site where vertical ice displacement is <5cm per day, and horizontal ice motion is <20 cm per day. A low-cost GNSS  
487 station installed within 600 m of glacier margin detected tidal horizontal oscillations of  $\pm 1$  cm. Such high-precision  
488 results will be reproducible in other study sites in Antarctica, providing that dual-frequency, multi-constellation  
489 receiver and antenna hardware is used.

490 The experiments presented here provide a ‘proof of concept’ of the efficacy of low-cost GNSS positioning systems  
491 for glaciological monitoring applications. The mass-market receivers and antennas evaluated here yield both a  
492 considerable cost advantage and a ~50% reduction in power consumption in comparison to a survey-grade system.  
493 These experiments encourage the widespread use of low-cost receivers to expand and densify GNSS monitoring  
494 networks, both in Antarctica and in glaciated regions worldwide.

## 495 8 SUPPLEMENTARY MATERIAL

496 The supplementary material for this article can be found at: XXXXXXXXXXXXXXX

## 497 9 DATA AND SOFTWARE

498 The long baseline positioning uses multi-GNSS observations from the International GNSS Service (IGS) station  
499 SCTB near Scott Base, maintained by LINZ (2023) and downloaded in RINEX 3 format from the European Space  
500 Agency (ESA) GNSS Science Support Centre: <https://gssc.esa.int/>. Daily multi-GNSS broadcast ephemeris files  
501 (BRDM00DLR product) (Steigenberger and Montenbruck, 2020) are from the CDDIS GNSS data archive (Noll,  
502 2010): [https://cddis.nasa.gov/Data\\_and\\_Derived\\_Products/GNSS/gnss\\_mgex.html](https://cddis.nasa.gov/Data_and_Derived_Products/GNSS/gnss_mgex.html). Final multi-GNSS precise  
503 orbit and clock information (Männel and others, 2022; Montenbruck and others, 2017) generated by the GFZ  
504 Analysis Centre are available from the Analysis Center of the Multi-GNSS Experiment (MGEX): <https://www.gfz-potsdam.de/en/section/space-geodetic-techniques/projects/mgex>. Global K<sub>p</sub> index values (Matzka and others, 2021)  
505 presented in Fig. 13 were downloaded from <https://kp.gfz-potsdam.de/en/data>. Modified Sentinel-2 images in Fig. 1  
506 were downloaded from <https://scihub.copernicus.eu/dhus/#/home>.  
507

508 The software u-center v22.07 is available at <https://www.u-blox.com/en/product/u-center>. The Trimble RINEX  
509 Converter ‘ConvertToRINEX v3.14.0’ software is available at <https://geospatial.trimble.com/trimble-rinex-converter>.  
510 Hatanaka-compressed RINEX files are uncompressed with the RNXCMP software available at: <https://terras.gsi.go.jp/ja/crx2rnx.html>. GNSS datasets were processed with the open-source software RTKLIB (v.2.4.3 b34, developed  
511 by T. Takasu), available at <https://rtklib.com/>. CSRS-PPP solutions (Banville and others, 2021) were generated  
512 with the online service: <https://webapp.csrs-scrs.nrcan.gc.ca/geod/tools-outils/ppp.php>. The CATS2008 tide  
513 model (Padman and others, 2002; Howard and others, 2019) used to generate the prediction in Figs. 11 and 12, is  
514 available at <https://www.usap-dc.org/view/dataset/601235>.  
515

## 516 10 CODE AVAILABILITY

517 A description of the low-cost GNSS hardware components and data logger code is available on GitHub (<https://github.com/hollystill/L>

## 518 11 ACKNOWLEDGEMENTS

519 HS is supported by the Antarctica New Zealand Doctoral Scholarship and the University of Otago Doctoral Scholar-  
520 ship. The field campaign was supported by the Marsden Fund (grant number UOO052) awarded to DJP. We express  
521 our gratitude to Antarctica New Zealand and the staff at Scott Base for logistical support. We also express our  
522 appreciation to the staff at Mario Zucchelli Station for supporting both logistical and field operations, and for assis-  
523 tance to install a temporary base station. We thank Brent Pooley for fabricating the ground plates used for the patch

524 antennas, and the School of Surveying, University of Otago, for lending the Trimble GNSS equipment. The authors  
525 gratefully acknowledge T. Takasu for their contribution to developing the open-source GNSS processing software  
526 RTKLIB. We acknowledge the editor and three reviewers for their helpful feedback on the original manuscript.

## 527 12 AUTHOR CONTRIBUTIONS

528 HS and RO designed the research. MHB and HS built and configured the u-blox GNSS stations. HS, MHB and DJP  
529 collected the GNSS datasets. HS processed the GNSS data with support from RO. HS wrote the paper with support  
530 from CH, RO, MHB and DJP.

## 531 REFERENCES

- 532 Alkan RM, Erol S and Mutlu B (2022) Real-time multi-GNSS Precise Point Positioning using IGS-RTS products in Antarctic  
533 region. *Polar Science*, **32**, 100844 (doi: 10.1016/J.POLAR.2022.100844)
- 534 AllTerra (2023) GPS/GNSS Systems - Surveying Equipment - Products (Accessed:  
535 <https://allterracentral.com/products.html/survey-equipment/gps-systems.html>)
- 536 Arzeno IB, Beardsley RC, Limeburner R, Owens B, Padman L, Springer SR, Stewart CL and Williams MJ (2014) Ocean  
537 variability contributing to basal melt rate near the ice front of Ross Ice Shelf, Antarctica. *Journal of Geophysical Research: Oceans*, **119**, 4214–4233 (doi: 10.1002/2014JC009792)
- 539 Banville S, Hassen E, Lamothe P, Farinaccio J, Donahue B, Mireault Y, Goudarzi MA, Collins P, Ghoddousi-Fard R and  
540 Kamali O (2021) Enabling ambiguity resolution in CSRS-PPP. *Navigation*, **68**, 433–451 (doi: 10.1002/NAVI.423)
- 541 Brunt KM, Neumann TA and Larsen CF (2019) Assessment of altimetry using ground-based GPS data from the 88S Traverse,  
542 Antarctica, in support of ICESat-2. *Cryosphere*, **13**, 579–590 (doi: 10.5194/TC-13-579-2019)
- 543 Chagas AM (2018) Haves and have nots must find a better way: The case for open scientific hardware. *PLOS Biology*, **16**,  
544 e3000014 (doi: 10.1371/JOURNAL.PBIO.3000014)
- 545 Cooley J, Winberry P, Koutnik M and Conway H (2019) Tidal and spatial variability of flow speed and seismicity near the  
546 grounding zone of Beardmore Glacier, Antarctica. *Annals of Glaciology*, **60**, 37–44 (doi: 10.1017/aog.2019.14)
- 547 Dabave P, Linty N and Dovis F (2020) Analysis of multi-constellation GNSS PPP solutions under phase scintillations at high  
548 latitudes. *Applied Geomatics*, **12**, 45–52 (doi: 10.1007/s12518-019-00269-4)
- 549 den Ouden MA, Reijmer CH, Pohjola V, van De Wal RS, Oerlemans J and Boot W (2010) Stand-alone single-frequency GPS  
550 ice velocity observations on Nordenskiöldbreen, Svalbard. *Cryosphere*, **4**, 593–604 (doi: 10.5194/tc-4-593-2010)

- 551 Di M, Guo B, Ren J, Wu X, Zhang Z, Liu Y, Liu Q and Zhang A (2022) GNSS Real-Time Precise Point Positioning in Arctic  
552 Northeast Passage. *Journal of Marine Science and Engineering*, **10**, 1345 (doi: 10.3390/JMSE10101345)
- 553 Doherty PH, Delay SH, Valladares CE and Klobuchar JA (2003) Ionospheric scintillation effects on GPS in the equatorial and  
554 auroral regions. *Navigation*, **50**, 235–245 (doi: 10.1002/j.2161-4296.2003.tb00332.x)
- 555 GNSS OEM (2023) GNSS RTK Multiband Antennas: L1/L2/L5 GPS, G1/G2/G3 GLONASS, B1/B2/B3 BDS, Galileo  
556 E1/E5/E6 38dB Survey Antenna for RTK Base station. Available at: <https://gnss.store/gnss-rtk-multiband-antennas/140-elt0123.html> (Last accessed: August 20, 2023)
- 558 Greene CA, Gardner AS and Andrews LC (2020) Detecting seasonal ice dynamics in satellite images. *The Cryosphere*, **14**,  
559 4365–4378 (doi: 10.5194/tc-14-4365-2020)
- 560 Hamza V, Stopar B, Ambrožič T, Turk G and Sterle O (2020) Testing Multi-Frequency Low-Cost GNSS Receivers for Geodetic  
561 Monitoring Purposes. *Sensors*, **20**, 4375 (doi: 10.3390/S20164375)
- 562 Horgan HJ, Hulbe C, Alley RB, Anandakrishnan S, Goodsell B, Taylor-Offord S and Vaughan MJ (2017) Poststagnation  
563 Retreat of Kamb Ice Stream's Grounding Zone. *Geophysical Research Letters*, **44**, 9815–9822 (doi: 10.1002/2017GL074986)
- 564 Howard SL, Padman L and Erofeeva S (2019) CATS2008: Circum-Antarctic Tidal Simulation version 2008 (Accessed:  
565 <https://doi.org/10.15784/601235>)
- 566 Huang MH, Lopez KU and Olsen KG (2022) Icequake-Magnitude Scaling Relationship Along a Rift Within the Ross Ice Shelf,  
567 Antarctica. *Geophysical Research Letters*, **49**, e2022GL097961 (doi: 10.1029/2022GL097961)
- 568 Hugentobler U and Montenbruck O (2017) Satellite Orbits and Attitude. In Teunissen PJG and Montenbruck O (eds.),  
569 *Springer Handbook of Global Navigation Satellite Systems*, 1st edition. 59–90 (doi: 10.1007/978-3-319-42928-1)
- 570 Hulbe CL and Whillans IM (1994) Evaluation of strain rates on Ice Stream B, Antarctica, obtained using GPS phase mea-  
571 surements. *Annals of Glaciology*, **20**, 254–262 (doi: 10.3189/1994AoG20-1-254-262)
- 572 Hulbe CL and Whillans IM (1997) Weak bands within Ice Stream B, West Antarctica. *Journal of Glaciology*, **43**, 377–386  
573 (doi: 10.3189/S002214300003495X)
- 574 Hulbe CL, Klinger M, Masterson M, Catania G, Cruikshank K and Bugni A (2016) Tidal bending and strand cracks at the  
575 Kamb Ice Stream grounding line, West Antarctica. *Journal of Glaciology*, **62**, 816–824 (doi: 10.1017/jog.2016.74)
- 576 Johnston G, Riddell A and Hausler G (2017) The International GNSS Service. In Teunissen PJG and Montenbruck O (eds.),  
577 *Springer Handbook of Global Navigation Satellite Systems*, 1st edition. 967–982 (doi: 10.1007/978-3-319-42928-1)

- 578 Jones DH and Rose M (2015) Measurement of relative position of Halley VI modules (MORPH): GPS monitoring of building  
579 deformation in dynamic regions. *Cold Regions Science and Technology*, **120**, 56–62 (doi: 10.1016/j.coldregions.2015.09.010)
- 580 Jones DH, Robinson C and Gudmundsson GH (2016) A new high-precision and low-power GNSS receiver for long-term  
581 installations in remote areas. *Geoscientific Instrumentation, Methods and Data Systems*, **5**, 65–73 (doi: 10.5194/gi-5-65-  
582 2016)
- 583 King M (2004) Rigorous GPS data-processing strategies for glaciological applications. *Journal of Glaciology*, **50**, 601–607 (doi:  
584 10.3189/172756504781829747)
- 585 King M and Aoki S (2003) Tidal observations on floating ice using a single GPS receiver. *Geophysical Research Letters*, **30**,  
586 1138 (doi: 10.1029/2002GL016182)
- 587 King M, Nguyen LN, Coleman R and Morgan P (2000) Strategies for High Precision Processing of GPS Measurements with  
588 Application to the Amery Ice Shelf, East Antarctica. *GPS Solutions*, **4**, 2–12 (doi: 10.1007/PL00012824)
- 589 King MA, Watson CS and White D (2022) GPS Rates of Vertical Bedrock Motion Suggest Late Holocene Ice-Sheet Readvance  
590 in a Critical Sector of East Antarctica. *Geophysical Research Letters*, **49**, e2021GL097232 (doi: 10.1029/2021GL097232)
- 591 Klein E, Mosbeux C, Bromirski PD, Padman L, Bock Y, Springer SR and Fricker HA (2020) Annual cycle in flow of Ross Ice  
592 Shelf, Antarctica: contribution of variable basal melting. *Journal of Glaciology*, **66**, 861–875 (doi: 10.1017/JOG.2020.61)
- 593 Kouba J and Héroux P (2001) Precise Point Positioning Using IGS Orbit and Clock Products. *GPS Solutions*, **5**, 12–28 (doi:  
594 10.1007/PL00012883)
- 595 Krietemeyer A, van der Marel H, van de Giesen N and Veldhuis MCT (2022) A Field Calibration Solution to Achieve  
596 High-Grade-Level Performance for Low-Cost Dual-Frequency GNSS Receiver and Antennas. *Sensors*, **22**, 2267 (doi:  
597 10.3390/s22062267)
- 598 Linty N, Dovis F and Alfonsi L (2018) Software-defined radio technology for GNSS scintillation analysis: bring Antarctica to  
599 the lab. *GPS Solutions*, **22**, 96 (doi: 10.1007/s10291-018-0761-7)
- 600 LINZ (2023) PositioNZ | Toitū Te Whenua - Land Information New Zealand (Accessed: [https://www.linz.govt.nz/products-](https://www.linz.govt.nz/products-services/geodetic/positionz)  
601 [services/geodetic/positionz](https://www.linz.govt.nz/products-services/geodetic/positionz))
- 602 Manzini N, Orcesi A, Thom C, Brossault MA, Botton S, Ortiz M and Dumoulin J (2022) Performance analysis of low-cost  
603 GNSS stations for structural health monitoring of civil engineering structures. *Structure and Infrastructure Engineering*,  
604 **18**, 595–611 (doi: 10.1080/15732479.2020.1849320)
- 605 Maqsood M, Gao S and Montenbruck O (2017) Antennas. In Teunissen PJG and Montenbruck O (eds.), *Springer Handbook*  
606 *of Global Navigation Satellite Systems*, 1st edition. 505–534 (doi: 10.1007/978-3-319-42928-1)

- 607 Matzka J, Stolle C, Yamazaki Y, Bronkalla O and Morschhauser A (2021) The Geomagnetic Kp Index and Derived Indices  
608 of Geomagnetic Activity. *Space Weather*, **19**, e2020SW002641 (doi: 10.1029/2020SW002641)
- 609 Minowa M, Podolskiy EA and Sugiyama S (2019) Tide-modulated ice motion and seismicity of a floating glacier tongue in  
610 East Antarctica. *Annals of Glaciology*, **60**, 57–67 (doi: 10.1017/aog.2019.25)
- 611 Montenbruck O, Steigenberger P, Prange L, Deng Z, Zhao Q, Perosanz F, Romero I, Noll C, Stürze A, Weber G, Schmid  
612 R, MacLeod K and Schaer S (2017) The Multi-GNSS Experiment (MGEX) of the International GNSS Service (IGS) –  
613 Achievements, prospects and challenges. *Advances in Space Research*, **59**, 1671–1697 (doi: 10.1016/J.ASR.2017.01.011)
- 614 Männel B, Brandt A, Nischan T, Brack A, Sakic P and Bradke M (2022) GFZ final product series for  
615 the International GNSS Service (IGS) (doi: 10.5880/GFZ.1.1.2020.002) (Accessed: <https://dataservices.gfz-potsdam.de/panmetaworks/showshort.php?id=3e3bc33e-e137-11ea-9603-497c92695674>)
- 617 Nie W, Rovira-Garcia A, Li M, Fang Z, Wang Y, Zheng D and Xu T (2022) The Mechanism for GNSS-Based Kinematic  
618 Positioning Degradation at High-Latitudes Under the March 2015 Great Storm. *Space Weather*, **20**, e2022SW003132 (doi:  
619 10.1029/2022SW003132)
- 620 Nie Z, Liu F and Gao Y (2020) Real-time precise point positioning with a low-cost dual-frequency GNSS device. *GPS Solutions*,  
621 **24**, 9 (doi: 10.1007/s10291-019-0922-3)
- 622 Nievinski FG and Larson KM (2014) Inverse modeling of GPS multipath for snow depth estimation - Part I: Formulation and  
623 simulations. *IEEE Transactions on Geoscience and Remote Sensing*, **52**, 6555–6563 (doi: 10.1109/TGRS.2013.2297681)
- 624 NOAA (2023) Geomagnetic KP and AP Indices (Accessed: [https://www.ngdc.noaa.gov/stp/geomag/kp\\_ap.html](https://www.ngdc.noaa.gov/stp/geomag/kp_ap.html))
- 625 Noll CE (2010) The crustal dynamics data information system: A resource to support scientific analysis using space geodesy.  
626 *Advances in Space Research*, **45**, 1421–1440 (doi: 10.1016/J.ASR.2010.01.018)
- 627 Notti D, Cina A, Manzino A, Colombo A, Bendea IH, Mollo P and Giordan D (2020) Low-Cost GNSS Solution for Con-  
tinuous Monitoring of Slope Instabilities Applied to Madonna Del Sasso Sanctuary (NW Italy). *Sensors*, **20**, 289 (doi:  
629 10.3390/S20010289)
- 630 Odijk D and Wanninger L (2017) Differential Positioning. In Teunissen PJG and Montenbruck O (eds.), *Springer Handbook  
631 of Global Navigation Satellite Systems*, 1st edition. 753–780 (doi: 10.1007/978-3-319-42928-1)
- 632 Odolinski R (2012) Temporal correlation for network RTK positioning. *GPS Solutions*, **16**, 147–155 (doi: 10.1007/S10291-011-  
633 0213-0)
- 634 Odolinski R and Teunissen PJ (2016) Single-frequency, dual-GNSS versus dual-frequency, single-GNSS: a low-cost and high-  
635 grade receivers GPS-BDS RTK analysis. *Journal of Geodesy*, **90**, 1255–1278 (doi: 10.1007/S00190-016-0921-X)

- 636 Odolinski R and Teunissen PJ (2017a) Low-cost, 4-system, precise GNSS positioning: a GPS, Galileo, BDS and QZSS  
637 ionosphere-weighted RTK analysis. *Measurement Science and Technology*, **28**, 125801 (doi: 10.1088/1361-6501/AA92EB)
- 638 Odolinski R and Teunissen PJ (2017b) Low-cost, high-precision, single-frequency GPS–BDS RTK positioning. *GPS Solutions*,  
639 **21**, 1315–1330 (doi: 10.1007/s10291-017-0613-x)
- 640 Odolinski R and Teunissen PJ (2020) Best integer equivariant estimation: performance analysis using real data collected by  
641 low-cost, single- and dual-frequency, multi-GNSS receivers for short- to long-baseline RTK positioning. *Journal of Geodesy*,  
642 **94**, 1–17 (doi: 10.1007/S00190-020-01423-2)
- 643 Odolinski R, Odijk D and Teunissen PJ (2014) Combined GPS and BeiDou Instantaneous RTK Positioning. *Navigation*, **61**,  
644 135–148 (doi: 10.1002/NAVI.61)
- 645 Odolinski R, Teunissen PJ and Odijk D (2015a) Combined BDS, Galileo, QZSS and GPS single-frequency RTK. *GPS Solutions*,  
646 **19**, 151–163 (doi: 10.1007/S10291-014-0376-6)
- 647 Odolinski R, Teunissen PJ and Odijk D (2015b) Combined GPS + BDS for short to long baseline RTK positioning. *Measure-  
648 ment Science and Technology*, **26**, 045801 (doi: 10.1088/0957-0233/26/4/045801)
- 649 Oellermann M, Jolles JW, Ortiz D, Seabra R, Wenzel T, Wilson H and Tanner RL (2022) Open Hardware in Science: The  
650 Benefits of Open Electronics. *Integrative and Comparative Biology*, **62**, 1061–1075 (doi: 10.1093/ICB/ICAC043)
- 651 Padman L, Fricker HA, Coleman R, Howard S and Erofeeva L (2002) A new tide model for the Antarctic ice shelves and seas.  
652 *Annals of Glaciology*, **34**, 247–254 (doi: 10.3189/172756402781817752)
- 653 Paziewski J (2022) Multi-constellation single-frequency ionospheric-free precise point positioning with low-cost receivers. *GPS  
654 Solutions*, **26**, 1–11 (doi: 10.1007/S10291-021-01209-9)
- 655 Paziewski J and Wielgosz P (2017) Investigation of some selected strategies for multi-GNSS instantaneous RTK positioning.  
656 *Advances in Space Research*, **59**, 12–23 (doi: 10.1016/j.asr.2016.08.034)
- 657 Paziewski J, Høeg P, Sieradzki R, Jin Y, Jarmolowski W, Hoque MM, Berdermann J, Hernandez-Pajares M, Wielgosz P,  
658 Lyu H, Miloch WJ and Orús-Pérez R (2022) The implications of ionospheric disturbances for precise GNSS positioning in  
659 Greenland. *Journal of Space Weather and Space Climate*, **12**, 33 (doi: 10.1051/SWSC/2022029)
- 660 Pratap B, Dey R, Matsuoka K, Moholdt G, Lindbäck K, Goel V, Laluraj CM and Thamban M (2022) Three-decade spatial  
661 patterns in surface mass balance of the Nivlisen Ice Shelf, central Dronning Maud Land, East Antarctica. *Journal of  
662 Glaciology*, **68**, 174–186 (doi: 10.1017/JOG.2021.93)
- 663 Punzet S and Eibert TF (2023) Impact of Additional Antenna Groundplanes on RTK-GNSS Positioning Accuracy of UAVs.  
664 *Advances in Radio Science*, **20**, 23–28 (doi: 10.5194/ARS-20-23-2023)

- 665 Richter A, Popov SV, Fritsche M, Lukin VV, Matveev AY, Ekaykin AA, Lipenkov VY, Fedorov DV, Eberlein L, Schröder L,  
666 Ewert H, Horwath M and Dietrich R (2014) Height changes over subglacial Lake Vostok, East Antarctica: Insights from  
667 GNSS observations. *Journal of Geophysical Research: Earth Surface*, **119**, 2460–2480 (doi: 10.1002/2014JF003228)
- 668 Rignot E, Mouginot J and Scheuchl B (2016) *MEASUREs Antarctic Grounding Line from Differential Satellite Radar*  
669 *Interferometry, Version 2*. NASA National Snow and Ice Data Center Distributed Active Archive Center (doi:  
670 10.5067/IKBWW4RYHF1Q)
- 671 Romero-Andrade R, Trejo-Soto ME, Vega-Ayala A, Hernández-Andrade D, Vázquez-Ontiveros JR and Sharma G (2021)  
672 Positioning Evaluation of Single and Dual-Frequency Low-Cost GNSS Receivers Signals Using PPP and Static Relative  
673 Methods in Urban Areas. *Applied Sciences*, **11**, 10642 (doi: 10.3390/APP112210642)
- 674 Schröder L, Richter A, Fedorov DV, Eberlein L, Brovkov EV, Popov SV, Knöfel C, Horwath M, Dietrich R, Matveev AY,  
675 Scheinert M and Lukin VV (2017) Validation of satellite altimetry by kinematic GNSS in central East Antarctica. *Cryosphere*,  
676 **11**, 1111–1130 (doi: 10.5194/TC-11-1111-2017)
- 677 Schüler T (2006) Impact of systematic errors on precise long-baseline kinematic GPS positioning. *GPS Solutions*, **10**, 108–125  
678 (doi: 10.1007/S10291-005-0012-6)
- 679 Šegina E, Peternel T, Urbančič T, Realini E, Zupan M, Jež J, Caldera S, Gatti A, Tagliaferro G, Consoli A, González JR and  
680 Auflič MJ (2020) Monitoring Surface Displacement of a Deep-Seated Landslide by a Low-Cost and near Real-Time GNSS  
681 System. *Remote Sensing*, **12**, 3375 (doi: 10.3390/RS12203375)
- 682 Siegfried MR, Fricker HA, Carter SP and Tulaczyk S (2016) Episodic ice velocity fluctuations triggered by a subglacial flood  
683 in West Antarctica. *Geophysical Research Letters*, **43**, 2640–2648 (doi: 10.1002/2016GL067758)
- 684 Skone S, Knudsen K and Jong MD (2001) Limitations in GPS receiver tracking performance under ionospheric scintillation  
685 conditions. *Physics and Chemistry of the Earth, Part A: Solid Earth and Geodesy*, **26**, 613–621 (doi: 10.1016/S1464-  
686 1895(01)00110-7)
- 687 Spikes VB, Csathó BM and Whillans IM (2003) Laser profiling over Antarctic ice streams: Methods and accuracy. *Journal of*  
688 *Glaciology*, **49**, 315–322 (doi: 10.3189/172756503781830737)
- 689 Steigenberger P and Montenbruck O (2020) In Villiger A and Dach R (eds.), *Multi-GNSS Working Group Technical Report*  
690 2019. 219–229 (doi: 10.7892/BORIS.144003)
- 691 Still H, Hulbe C, Forbes M, Prior DJ, Bowman MH, Boucinhias B, Craw L, Kim D, Lutz F, Mulvaney R and Thomas RE  
692 (2022) Tidal modulation of a lateral shear margin: Priestley Glacier, Antarctica. *Frontiers in Earth Science*, **10**, 687 (doi:  
693 10.3389/feart.2022.828313)

- 694 Takasu T (2013) RTKLIB Ver. 2.4.2 Manual: RTKLIB: An Open Source Program Package for GNSS Positioning (Accessed:  
695 [https://www.rtklib.com/prog/manual\\_2.4.2.pdf](https://www.rtklib.com/prog/manual_2.4.2.pdf))
- 696 Takasu T and Yasuda A (2009) Development of the low-cost RTK-GPS receiver with an open source program package RTKLIB.  
697 *International symposium on GPS/GNSS.*, **1**, 1–6 (doi: [https://gpspp.sakura.ne.jp/paper2005/isgps\\_2009\\_rklib.pdf](https://gpspp.sakura.ne.jp/paper2005/isgps_2009_rklib.pdf))
- 698 Teunissen PJ and Verhagen S (2009) The GNSS ambiguity ratio-test revisited: A better way of using it. *Survey Review*, **41**,  
699 138–151 (doi: 10.1179/003962609X390058)
- 700 Teunissen PJG (2017) Carrier Phase Integer Ambiguity Resolution. In Teunissen PJG and Montenbruck O (eds.), *Springer  
701 Handbook of Global Navigation Satellite Systems*, 1st edition. 661–685 (doi: 10.1007/978-3-319-42928-1)
- 702 Teunissen PJG, Odolinski R and Odijk D (2014) Instantaneous BeiDou+GPS RTK positioning with high cut-off elevation  
703 angles. *Journal of Geodesy*, **88**, 335–350 (doi: 10.1007/s00190-013-0686-4)
- 704 Thomas ID, King MA, Bentley MJ, Whitehouse PL, Penna NT, Williams SD, Riva RE, Lavallee DA, Clarke PJ, King EC,  
705 Hindmarsh RC and Koivula H (2011) Widespread low rates of Antarctic glacial isostatic adjustment revealed by GPS  
706 observations. *Geophysical Research Letters*, **38** (doi: 10.1029/2011GL049277)
- 707 Thomas RE, Negrini M, Prior DJ, Mulvaney R, Still H, Bowman MH, Craw L, Fan S, Hubbard B, Hulbe C, Kim D and Lutz  
708 F (2021) Microstructure and Crystallographic Preferred Orientations of an Azimuthally Oriented Ice Core from a Lateral  
709 Shear Margin: Priestley Glacier, Antarctica. *Frontiers in Earth Science*, **9**, 1084 (doi: 10.3389/feart.2021.702213)
- 710 Tidey E and Odolinski R (2023) Low-cost multi-GNSS, single-frequency RTK averaging for marine applications: accurate  
711 stationary positioning and vertical tide measurements. *Marine Geodesy*, **46**, 333–358 (doi: 10.1080/01490419.2023.2208289)
- 712 Tunini L, Zuliani D and Magrin A (2022) Applicability of Cost-Effective GNSS Sensors for Crustal Deformation Studies.  
713 *Sensors*, **22**, 350 (doi: 10.3390/S22010350)
- 714 U-blox (2019) GNSS antennas: RF design considerations for u-blox GNSS receivers. Available at: [https://content.u-blox.com/sites/default/files/products/documents/GNSS-Antennas\\_AppNote\\_%28UBX-15030289%29.pdf](https://content.u-blox.com/sites/default/files/products/documents/GNSS-Antennas_AppNote_%28UBX-15030289%29.pdf) (Last accessed:  
715 1 June, 2023)
- 716 U-blox (2022a) ANN-MB series multi-band, high precision GNSS antennas. Available at: [https://content.u-blox.com/sites/default/files/documents/ANN-MB\\_DataSheet\\_UBX-18049862.pdf](https://content.u-blox.com/sites/default/files/documents/ANN-MB_DataSheet_UBX-18049862.pdf) (Last accessed: 1 June, 2023)
- 717 U-blox (2022b) U-center GNSS evaluation software for Windows. Available at: [https://content.u-blox.com/sites/default/files/u-center\\_Userguide\\_UBX-13005250.pdf](https://content.u-blox.com/sites/default/files/u-center_Userguide_UBX-13005250.pdf) (Last accessed: 1 June, 2023)
- 718 U-blox (2022c) ZED-F9P-04B u-blox F9 high precision GNSS module. Available at: [https://content.u-blox.com/sites/default/files/ZED-F9P-04B\\_DataSheet\\_UBX-21044850.pdf](https://content.u-blox.com/sites/default/files/ZED-F9P-04B_DataSheet_UBX-21044850.pdf) (Last accessed: 1 June, 2023)

- 723 U-blox (2023) ZED-F9P module | u-blox. Available at: <https://www.u-blox.com/en/product/zed-f9p-module> (Last accessed:  
724 1 June, 2023)
- 725 Verhagen S and Teunissen PJ (2013) The ratio test for future GNSS ambiguity resolution. *GPS Solutions*, **17**, 535–548 (doi:  
726 10.1007/s10291-012-0299-z)
- 727 Wanninger L and May M (2001) Carrier-phase multipath calibration of GPS reference stations. *Navigation*, **48**, 112–124 (doi:  
728 10.1002/j.2161-4296.2001.tb00233.x)
- 729 Willis MJ (2008) Technologies to Operate Year-Round Remote Global Navigation Satellite System (GNSS) Stations in Extreme  
730 Environments. In Capra A and Dietrich R (eds.), *Geodetic and Geophysical Observations in Antarctica*, 1st edition. 11–35  
731 (doi: 10.1007/978-3-540-74882-3\_2)
- 732 Xue C, Psimoulis P, Zhang Q and Meng X (2021) Analysis of the performance of closely spaced low-cost multi-GNSS receivers.  
733 *Applied Geomatics*, **13**, 415–435 (doi: 10.1007/S12518-021-00361-8)
- 734 Xue C, Psimoulis PA and Meng X (2022) Feasibility analysis of the performance of low-cost GNSS receivers in monitoring  
735 dynamic motion. *Measurement*, **202**, 111819 (doi: 10.1016/J.MEASUREMENT.2022.111819)
- 736 Yong C, Odolinski R, Zaminpardaz S, Moore M, Rubinov E, Er J and Denham M (2021) Instantaneous, Dual-Frequency,  
737 Multi-GNSS Precise RTK Positioning Using Google Pixel 4 and Samsung Galaxy S20 Smartphones for Zero and Short  
738 Baselines. *Sensors*, **21**, 8318 (doi: 10.3390/S21248318)
- 739 Zanutta A, Negusini M, Vittuari L, Cianfarra P, Salvini F, Mancini F, Sterzai P, Dubbini M, Galeandro A and Capra A (2017)  
740 Monitoring geodynamic activity in the Victoria Land, East Antarctica: Evidence from GNSS measurements. *Journal of  
741 Geodynamics*, **110**, 31–42 (doi: 10.1016/J.JOG.2017.07.008)
- 742 Zanutta A, Negusini M, Vittuari L, Martelli L, Cianfarra P, Salvini F, Mancini F, Sterzai P, Dubbini M and Capra A (2018)  
743 New Geodetic and Gravimetric Maps to Infer Geodynamics of Antarctica with Insights on Victoria Land. **10**, 1608 (doi:  
744 10.3390/rs10101608)
- 745 Zhang Q, Chen Z, Cui Y, Zheng X, Rong F, Sun Y and Gao L (2020) A refined metric for multi-GNSS constellation availability  
746 assessment in polar regions. *Advances in Space Research*, **66**, 655–670 (doi: 10.1016/J.ASR.2020.04.033)
- 747 Zumberge JF, Heflin MB, Jefferson DC, Watkins MM and Webb FH (1997) Precise point positioning for the efficient and  
748 robust analysis of GPS data from large networks. *Journal of Geophysical Research: Solid Earth*, **102**, 5005–5017 (doi:  
749 10.1029/96JB03860)